Article

Not peer-reviewed version

mRNA-Based Solution for 47, 48, 51, and 52 Dystrophin Exon Deletions: DMD Patient-Donate Primer Cells (In Vitro) and Transgenic Mice Experimental Study (In Vivo)

Ali Taghizadehghalehjoughi *, Sidika Genc, Kubra Karabulut, Esmanur Nigde, Serkan Yildirim, Metin Kılıclıoglu, Damla Gul Findik, Erhan Şahin, Ramazan Çınar, Demet Celebi, Ozgur Celebi, Betul Ari, Sumeyye Baser

Posted Date: 9 April 2026

doi: 10.20944/preprints202511.0016.v2

Keywords: DMD; exon deletion; mRNA; mdx/d2

 doi:10.20944/preprints202511.0016.v2

Article

mRNA-Based Solution for 47, 48, 51, and 52 Dystrophin Exon Deletions: DMD Patient-Donate Primer Cells (In Vitro) and Transgenic Mice Experimental Study (In Vivo)

Ali Taghizadehghalehjoughi [1,*], Sidika Genc [1], Kubra Karabulut [1], Esmanur Nigde [1], Serkan Yildirim [2,3], Metin Kilicoglu [2], Damla Gul Findik [4], Erhan Sahin [5], Ramazan Cinar [6], Demet Celebi [7], Ozgur Celebi [8], Betul Ari [9] and Sumeyye Baser [10]

[1] Department of Medical Pharmacology, Faculty of Medicine, Bilecik Şeyh Edebali University, 11230, Bilecik, Türkiye
[2] Department of Pathology, Faculty of Veterinary Medicine, Atatürk University, 25240, Erzurum, Türkiye
[3] Department of Pathology, Faculty of Veterinary Medicine, Kyrgyz Turkish Manas University, Bishkek, Kyrgyzstan
[4] Department of Histology and Embryology, Faculty of Medicine, Balıkesir University, 10145, Balıkesir, Türkiye
[5] Department of Histology and Embryology, Faculty of Medicine, Bilecik Şeyh Edebali University, 11230 Bilecik, Türkiye
[6] Department of Biophysics, Faculty of Medicine, Bilecik Şeyh Edebali University, 11230 Bilecik, Turkey
[7] Department of Microbiology, Faculty of Veterinary Medicine, Atatürk University, 25240 Erzurum, Türkiye
[8] Department of Medical Microbiology, Faculty of Medicine, Atatürk University, 25240 Erzurum, Türkiye
[9] Department of Molecular Biology and Genetics, Faculty of Science, Atatürk University, 25240 Erzurum, Türkiye
[10] Department of Pharmaceutical Microbiology, Faculty of Pharmacy, 24002, Erzincan, Turkey
* Correspondence: ali.tgzd@bilecik.edu.tr

Abstract

Background/Objectives: Duchenne muscular dystrophy (DMD) is a genetic disorder caused by mutations in the dystrophin gene. DMD is characterized by exon deletions in about 76% of cases, with common deletions in exons 47, 48, 51, and 52. We evaluated the effectiveness of an mRNA-based therapy targeting these exon deletions, which are frequently seen in DMD patients. **Methods**: The current study involved two protocols: 1. applying the therapy to cells from patients diagnosed with DMD, and 2. applying the therapy to genetically modified transgenic mdx/d2 mice. After treatment, dystrophin was detected in all experimental groups. **Results**: Our study showed that, both in vitro and in vivo analyses demonstrated that the mRNA-based therapy successfully restored dystrophin expression in dystrophic muscle cells and tissues. Gene expression analysis, together with protein-level assessments, including Western blot, immunofluorescence (IF), ELISA, and immunohistochemistry (IHC), confirmed a significant increase in dystrophin levels in the treated groups compared with the control group. In addition to dystrophin restoration, other key sarcolemmal proteins involved in maintaining muscle membrane stability, such as γ-sarcoglycan, β-dystroglycan, and β-actin, were also highly expressed. These findings suggest an overall improvement in muscle cell membrane integrity. Consistent with the molecular results, behavioral analyses performed in the animal model revealed significant functional improvements, including enhanced mobility, motor coordination, longer walking and resting durations, and a reduced risk of falls. Overall, the results indicate that mRNA-mediated dystrophin replacement improves both muscle structural integrity and functional performance. **Conclusions:** Our study proved that the mRNA complex successfully produced functional dystrophin in transgenic mdx/d2 mice without causing allergic reactions or damage to the kidney, intestines, muscles, or brain.

 doi:10.20944/preprints202511.0016.v2

Keywords: DMD; exon deletion; mRNA; mdx/d2

1. Introduction

The dystrophin gene is the largest in the human genome, comprising 79 exons and encoding the 427 kDa dystrophin protein. Functionally, dystrophin is an essential cytoskeletal protein located on the inner surface of the muscle cell membrane and is concentrated at sites of cell-cell contact [1]. In muscle, dystrophin is an essential part of the dystrophin-glycoprotein complex (DGC), and the associated glycoprotein complex includes dystroglycan, sarcoglycan, sarcospan, and laminin [2]. Dystroglycan consists of two subunits, α and β. α-Dystroglycan, an extracellular peripheral membrane protein and laminin-2 receptor, anchors the DGC to the extracellular matrix (ECM). Sarcoglycans form a tight complex with sarcospan, strengthening the connection between α- and β-dystroglycans. In addition to its structural role, the sarcoglycan-sarcospan subcomplex also contributes to signal transduction and mechanoprotection [3]. This entire complex is essential for muscle physiology and function. However, the absence of dystrophin results in the complete loss of the dystrophin-associated protein complex and leads to membrane-fragility disorders [4]. Dystrophin-associated disorders include Duchenne Muscular Dystrophy (DMD). Exon deletions account for 60-70% of cases in DMD, whereas frameshift mutations and duplications account for 30-40% [5]. The most common hotspot for exon deletions in DMD is located in the core of dystrophin, between exons 45 and 55 [6]. In particular, the central region is nearly indispensable in function and is the source of genetic pathology in DMD.

In DMD, these mutations lead to premature termination of protein translation and inhibit dystrophin production [7]. Muscle weakness results from the absence of the dystrophin protein. Early signs include trouble climbing stairs, difficulty walking without support, and frequent falls; these usually appear between ages 2 and 3. Most patients become wheelchair-dependent between the ages of 10 and 12 and need respiratory support by around age 20. With proper care, many with DMD die from heart or lung failure between the ages of 20 and 40 [5,8]. Dystrophin is mainly expressed in skeletal and cardiac muscle. However, it has also been found in the brain, liver, intestine, kidney, and retina. Its presence in the brain is less extensive than in the muscles, which helps explain some of the central nervous system symptoms of the disease [9]. For example, there is a decline in learning ability, impaired muscle coordination, and degeneration of both afferent and efferent nerves. Epilepsy occurs more frequently than in the general population, and autism-like behaviors have been occasionally observed [10]. It is known that ALT and AST enzymes, in particular, are characteristically elevated in the liver [11]. Problems such as constipation caused by muscle weakness have been reported in the gastrointestinal tract [12]. Studies have indicated that cysteine levels in the kidneys are increased in DMD [13]. These studies have demonstrated that renal involvement is linked to chronic cardiac dysfunction, low water intake, and diuretic use [14]. Long-term follow-up studies have shown that although myofibrillar atrophy, necrosis, and fatty degeneration are observed in patients with DMD, endomysial fibrosis remains the standard myopathological parameter for reflecting the severity of pathology [15]. Various studies have shown that the healing capacity of muscle tissue is limited relative to other tissues. Fibrosis formation and ongoing myofibrillar destruction cannot be fully offset by satellite cell proliferation. The inflammatory process that follows muscle necrosis leads to the formation of fibrotic tissue and the replacement of fatty tissue [16].

Although the molecular basis of the disease is well-defined, the limited number of preclinical models that accurately reflect the complex pathophysiology of human DMD makes it challenging to develop new treatment strategies. A significant portion of preclinical studies conducted for this purpose are based on the mdx (B10.mdx) mouse model, which carries a nonsense mutation in exon 23 of the DMD gene and is reared on a C57BL/10 genetic background. However, this model exhibits a significantly milder phenotype than the human disease; limited muscle degeneration, minimal fibrosis, and relatively mild functional impairment reduce the translational value of DMD treatments.

 doi:10.20944/preprints202511.0016.v2

Studies aimed at overcoming these limitations have shown that the D2.mdx model, created by transferring the mdx mutation to the DBA/2J genetic background, exhibits pathological severity more closely resembling that of human DMD. D2.mdx mice are characterized by significantly increased muscle damage, impaired muscle regeneration, severe muscle atrophy, and rapidly progressing intramuscular fibrosis compared to B10.mdx mice of the same age group. Furthermore, the more severe phenotype observed in this model has been reported to be associated with a hyperfibrotic polymorphism in latent TGFβ-binding protein (LTBP). It has been shown that the same polymorphism plays a decisive role as a genetic modifier in disease progression in DMD patients. Therefore, the D2.mdx model is increasingly regarded as a valuable, clinically relevant small-animal model for translational DMD research.

In our study, the preference for the D2.mdx model, given its pathophysiology more closely resembles human DMD, enables a more realistic clinical evaluation of the findings. The pronounced fibrotic response, impaired regenerative capacity, and severe muscle degeneration in this model helped us to more sensitively and meaningfully reveal the effects of the mechanisms or therapeutic agents targeted by our study. Therefore, the use of D2.mdx mice constitutes the fundamental methodological basis of our research, both for more accurately elucidating pathological processes and for increasing the translational validity of potential treatments. Accordingly, our study aims to evaluate the therapeutic effects of the mRNA-based treatment approach we developed for exon 47, 48, 51, and 52 deletions on the D2.mdx mouse model and to comprehensively elucidate the molecular and functional responses elicited by this treatment in DMD patient-derived primary cells (in vitro) and in the D2.mdx model (in vivo).

2. Materials and Methods

2.1. Pre-Experimental Stages and Patent Process

Patent applications have been filed for mRNA transporter complexes in exons 52, 51, 48, and 47 (Application No: 25/002849, Reference No: 21428/5). In this study, we examined the results of the patented mRNA transporter complexes for exons 52, 51, 48, and 47, which have limited detail (sequences and release data).

2.2. Experimental Design

The study was designed in two steps. A. In vitro (patient donated cells n=6), and B. In vivo (transgenic mice mdx/d2 n=60) (Figure 1).

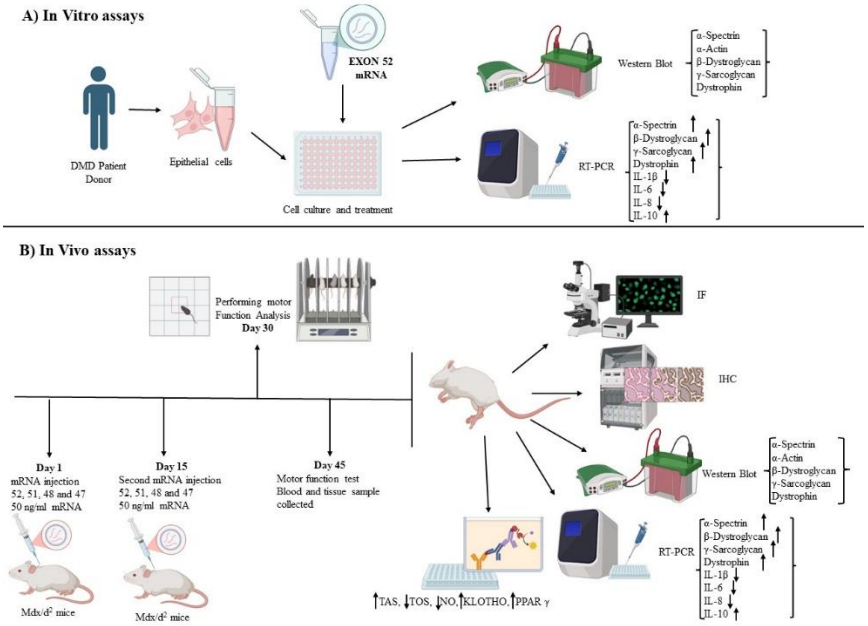

 doi:10.20944/preprints202511.0016.v2

Figure 1. A) In vitro analysis: Primary cells were collected from DMD patients. A primer cell was used to select an effective mRNA sequence. B) In vivo analysis was performed on mdx/d2 mice: mRNA from exons 52, 51, 48, and 47 was tested in primary isolated cells.

2.3. In Vitro Evaluation of Exon 52 Targeted mRNA Construction

This study evaluated the suitability and optimal sequencing of mRNA constructs targeting exon 52, using three different promoter regions and poly(A) tails, for patients with DMD (Table 1). In vitro analyses were performed to determine the transcriptional integrity, intracellular expression potential, and sequencing accuracy of the generated mRNAs. In this context, because there are no in vitro models that directly reflect DMD, myocytes were collected from individuals with DMD under ethical permission number 218345 from the Bilecik Şeyh Edebali University Ethics Committee to evaluate cellular transfection efficiency and mRNA stability. The cells were cultured under standard conditions and, once they reached the appropriate density, were individually transfected with three different exon 52 mRNA constructions. After 72 hours of transfection, the cells were harvested, and total RNA was isolated.

In the RNA samples obtained, the correct sequencing and integrity of the transfected mRNAs were confirmed by reverse transcription-polymerase chain reaction (RT-PCR) and sequence analysis. In addition, the functional efficacy of promoter regions and poly(A) tails was comparatively evaluated based on mRNA expression levels. As a result of these analyses, mRNA constructions with the highest applicability and confirmed sequencing accuracy for DMD patients were determined.

Table 1. Exon deletions and base sequences used for in vitro analyses.

Groups	Seq. Lengths
EX52-1	556
EX52-2	586
EX52-3	921

2.3.1. Cell Culture

Myocyte cells from 6 patients with DMD were cultured in fresh DMEM (Sigma, USA). Experimental groups included: Positive Control (healthy individual cells), Negative Control (DMD patient myocyte cells), and various exon 52 sequences (Table 1) (n=8). The in vitro experiment lasted 24 hours. At the end of the study, immunohistochemistry and RT-PCR were performed.

2.3.2. Real-Time PCR

Total RNA was extracted from cell samples using an RNA isolation kit (EcoTech, TRY271224). RNAs obtained from cells were used for cDNA synthesis (ThermoFisher, 2979096). All steps were carried out according to the manufacturer's instructions. Subsequently, the gene expression levels of α-spectrin, β-dystroglycan, γ-sarcoglycan, and dystrophin were normalized to β-actin, and three replicates were performed for each gene set.

2.4. Animal Studies and Ethical Considerations

All animal experiments conducted in this study were approved by the Acıbadem Mehmet Ali Aydınlar University Local Ethics Committee for Animal Experiments. The study was conducted under ethical approval number ACU-HADYEK-2024/51, obtained on July 24, 2024. The experiments were performed in accordance with relevant national and international animal welfare and ethical guidelines.

Based on mRNA constructions whose correct sequence and functional suitability were confirmed by PCR and IHC analyses, novel mRNA designs targeting exons 47, 48, 51, and 52, encompassing the exon deletions frequently seen in Duchenne Muscular Dystrophy, were created. In this design process, the previously validated exon 52 promoter region and poly(A) tail were

 doi:10.20944/preprints202511.0016.v2

preserved, and only the target exon sequences were rearranged, creating separate mRNA constructions for each exon.

2.4.1. Experimental Protocol

To evaluate the in vivo efficacy of the prepared exon 47-, 48-, 51-, and 52-targeted mRNAs, five experimental groups were established (n=12). Using transgenic mdx/D2 mice (from Jackson Laboratory, USA) that model DMD pathophysiology, animals were grouped by targeted exon. Each experimental group received the mRNA construct targeting the relevant exon, while the control group received no treatment. Animals were injected intramuscularly with 100 µL of the Exon-mRNA complex (in saline) on days 0 and 15. The experimental duration was 45 days.

2.5. Assessment of Behavioral Activity

2.5.1. Rotarod Test

Mice that had been treated with the Exon-mRNA complex were required to train on a rotating bar. Circular plastic coils with a diameter of 30 mm were restricted to 7.5 cm sections of the rotating bar for each mouse. The rotation speed was four revolutions per minute. The animals walked on the rotating bar for 4 minutes at the beginning and end of the experiment. The rotation speed was set to 18 rpm [17]. The mouse was placed on the rotating bar with its head oriented away from the rotation axis, and the timer was started. If the mouse fell, the time measurement was automatically interrupted. The mouse was then returned to the rotating bar, and time measurement resumed. This procedure was repeated until the total time spent walking on the rotating bar reached 200 seconds. The time to the first fall and the number of falls were recorded in both the control group and the mice treated with the Exon mRNA complex [18].

2.5.2. Administration of the Open Field Test

Forty-five days after treatment with the exon-mRNA complex, D2.mdx mice were tested on an activity monitor. The test was performed in an open-field arena (44 × 44 cm, Med Associates, St. Albans, VT) equipped with infrared light sensors (at 1.5 cm intervals) that detect horizontal and vertical activity (1.5 and 6 cm above ground level, respectively). The lighting in the center of the arena was ~150 lx. The arena floor was made of white plastic and covered with a black rubber layer where necessary. Animals were placed in the corners of the arena and monitored for 30 minutes. Distance traveled, number of stand-ups, and time spent in the corners (6 × 6 cm) and the central area (18 × 18 cm) were measured [19].

2.6. Sample Preparation

All mice were euthanized with a high dosage (50 mg/kg) of sodium thiopental anesthesia. Tissues, including skeletal muscle, heart, intestinal tissues, kidney, and brain, were procured for pathological examination and preserved in 10% formaldehyde. Muscle tissue was dissected and homogenized via PBS for real-time PCR (RT-PCR) and biochemical investigations, followed by centrifugation at 3000× g for 7 minutes at 4 °C. Supernatants were preserved at -86 °C until required.

2.6.1. Measurement of Oxidative Stress, Klotho, and PPARγ Protein Levels

This study evaluated α-Klotho, PPAR-γ, and oxidative stress markers at the protein level to elucidate the multifaceted effects of mRNA-based therapy on the pathophysiology of Duchenne Muscular Dystrophy (DMD)[20]. Muscle degeneration in DMD is not limited to dystrophin deficiency but is closely associated with chronic inflammation, fibrosis, and increased oxidative stress. Therefore, the selected markers were considered critical biological indicators of the disease's fundamental pathophysiology. For this purpose, the tissue samples were homogenized, lysed in cell lysis buffer, and centrifuged at 1500 rpm for 5 minutes. After centrifugation, the supernatant was

 doi:10.20944/preprints202511.0016.v2

collected for ELISA testing and stored at -20 °C until further analysis. Analyses were conducted following the protocols of the commercially available ELISA kit. The parameters tested included TAC (Rel Assay Diagnostic, TZ24152A), TOS (Rel Assay Diagnostic, 0K251770), α-klotho (BT Lab, 202408010), PPARγ (BT Lab, 202408010), and NO (BT Lab, 202208002). Each experiment used 15 mg of tissue. All analyses were performed in triplicate.

2.6.2. Gene Expression

Total RNA was extracted from homogenized tissue using an RNA isolation kit (EcoTech, TRY271224). RNAs obtained from muscle tissues were used for cDNA synthesis (ThermoFisher, 2979096). All steps were carried out according to the manufacturer's instructions. Subsequently, the gene expression levels of IL-1, IL-6, IL-8, IL-10, α-actin, α-spectrin, β-dystroglycan, γ-sarcoglycan, and dystrophin were measured in triplicate.

For the genes, 3 µl of primer/probe mix, 3 µl of cDNA, 10 µl of master mix, and 4 µl of distilled water were added to each tube. The final volume was adjusted to 20 µl. Forty-five cycles were performed after 600 seconds at 95 °C, 10 seconds at 95 °C, and 30 seconds at 60 °C. The expression levels of IL-1, IL-6, IL-8, IL-10, α-actin, α-spectrin, β-Dystroglycan, γ-sarcoglycan, and dystrophin were detected.

Table 2. Probe sequences of analyzed genes.

IL-1	**F:** ATGGCAACTGTCCCTGAACT **R:** AGTGACACTGCCTTCCTGAA
IL-6	**F:** TTGTCAAGACATGCCAAAGTGCTGA **R:** TGAGGGTGGGGCCAGAGC
IL-8	**F:** CATTAATATTTAACGATGTGGATGCGTTTCA **R:** GCCTACCATCTTTAAACTGCACAAT
IL-10	**F:** GCAGGACTTTAAGGGTTACTTGG **R:** GGGGAGAAATCGATGACAGC
α-Spectrin	**F:** TGCGCTGGAGAAGCTTACTG **R:** TGGTGTCAGAAGCTGTCTGG
γ-Sarcoglycan	**F:** GTGTCTATCCCAGATTTGG **R:** ACCACCCCTAAATCCTGCC
β-Dystroglycan	**F:** CTAGGATCCCACACAGTCATTCCG **R:** CTCGGATCCTTAAAGGGTAAGCTTGC
Dystrophin	**F:** ATCCTTGAATCCCACCATAAT **R:** CAGCAGAAATGAAAGGTAATATAGGA
β-Actin	**F:** CAGCCTTCCTTCTTGGGTATG **R:** AGCTCAGTAACAGTCCGCCT

2.6.3. Western Blot

Tissues were fragmented following a standard western blot protocol. A bicinchoninic acid (BCA) assay kit (Pierce, Rockford, IL, USA) was used to determine the concentrations of proteins in the lysate obtained from the tissues. Each well of an SDS-PAGE gel was loaded with an equal amount of buffer loading. 15 µL of sample was loaded into each well for Western blot analysis. After this process, the proteins on the gels were transferred to a nitrocellulose membrane. The membrane was then incubated for 1.5 hours with 3-5% non-fat milk powder to bind non-specific regions. After incubation, the membrane was washed three times for 5 minutes with TBST washing solution. Subsequently, dystrophin (sc-33697, 1:1000), α-dystroglycan (sc-53987, 1:1000), β-sarcoglycan (sc-

 doi:10.20944/preprints202511.0016.v2

100956, 1:1000), and β-actin (sc-47778, 1:1000) antibodies were incubated overnight. Appropriate secondary antibodies for the primer were diluted in 5% milk powder (mouse secondary antibody: 1/5000, mouse secondary antibody: 1/10,000), and the membranes were incubated with these antibodies for 1.5 hours. The membranes were treated with chemiluminescent conjugate (ECL). Band images were acquired using a SYNGENE G:Box Chemi XRQ imaging device. Band intensities in the acquired images were measured using ImageJ software. Protein expression levels were normalized to beta-actin, used as an internal control, and expressed as a percentage of the control [21].

2.6.4. Histochemical Analysis

After sacrifice, skeletal muscle tissue was fixed with 10% formaldehyde. Following fixation, the tissues were processed routinely and embedded in paraffin. 4 μm thick sections obtained from the paraffin blocks were placed on pre-prepared slides and deparaffinized. The sections were then stained using the hematoxylin-eosin (H&E) staining protocol. After staining, the sections were partially dried by dehydration in a rising alcohol series and then cleared with xylene and covered with a coverslip. To examine the general morphology of the tissues, the prepared sections were photographed for evaluation under a light microscope (Olympus CX23, Olympus EP50 camera, 1920 × 1080 pixels).

2.6.5. IHC (Immunohistochemical) Analysis

Antigen retrieval was performed at high temperature using citrate buffer (pH 6). Following retrieval, incubation with 3% hydrogen peroxide for 15 minutes was performed to inhibit endogenous peroxidase activity. After dropping the block solution onto the blocking slides, primary antibodies (Anti-dystrophin, 1:100; Anti-spectrin, 1:50; Anti-dystroglycan, 1:100; Anti-sarcoglycan, 1:100, Santa Cruz Biotechnology, Inc., Dallas, TX, USA) were incubated at room temperature for 1 hour. Subsequently, samples were washed with PBS for 15 minutes, and the HRP Detection System (Epredia, UltraVision Detection System) was applied. After incubation with the biotinylated secondary antibody and the streptavidin-peroxidase complex, DAB (Epredia, AEC chromogen kit) was applied as a chromogen for 1.5 minutes. Slides were counterstained with Harris hematoxylin. Immunoreactivity was assessed by optical density; each slide was analyzed in five randomly selected areas at x40 magnification (Xie Z et al., 2024). Slides were photographed with a light microscope (Olympus CX23, Olympus EP50 camera, 1920 × 1080 pixels), and protein expression was measured using ImageJ software. Area fraction (%) was used as a measure of immunoreactivity [22].

2.6.6. IF (Immunofluorescence) Analysis

5 μm sections were prepared on polylysine slides, deparaffinized, dehydrated, and then washed with PBS. To inhibit endogenous peroxidase activity, the sections were incubated in 3% hydrogen peroxide for 10 minutes. To prevent antigen masking in the nucleus, the sections were heated in a microwave oven for 5 minutes each, four times, in an antigen-retrieval solution (citrate buffer, pH 6). After microwave treatment, the sections were cooled to room temperature. While still in the solution, the sections were washed with PBS without removing them. Protein blocking was applied to the tissues. Primary antibodies (FITC, DAPI, TEXAS RED) were incubated in a humidified chamber for the times recommended in the antibody package insert, followed by a final PBS wash. Immunofluorescence antibody (FITC) was added at a 1:50 dilution and incubated in the dark for 45 minutes. A mixture of 9 parts distilled water and 1 part glycerol was applied to the tissues, covered with a coverslip, and examined under a fluorescence microscope (enter microscope brand) [23].

2.6.7. Statistical Analysis

GraphPad Prism 8.0.2 was used to perform statistical analysis of histopathological examinations, with $p < 0.05$ as the threshold for significance. The Duncan test was employed for intergroup comparisons. The nonparametric Kruskal-Wallis test assessed group differences, while the Mann-

 doi:10.20944/preprints202511.0016.v2

Whitney U test evaluated differences between groups. To determine the intensity of positive staining from images obtained through immunofluorescence staining, five random fields from each image were selected and analyzed using ZEISS Zen Imaging Software. Data were presented as the mean ± standard deviation (mean ± SD) for area percentage. A one-way ANOVA followed by Tukey's test was used to compare positive immunoreactive cells and immunopositive-stained areas with those in healthy controls. A $p<0.05$ was considered significant. Data are shown as mean ± SD.

3. Results

3.1. In Vitro Evaluation of Exon 52 Targeted mRNA Construction

3.1.1. Real-Time PCR Results

Upon evaluation, gene expression levels were significantly higher in the EX-1 and EX-3 groups than in the other groups. Although a statistically significant increase in gene levels was observed in the EX-2 group, this increase was lower than in the EX-1 and EX-3 groups. All gene expression data were normalized to the β-actin reference gene, analyses were performed in triplicate, and results were evaluated using mean values.

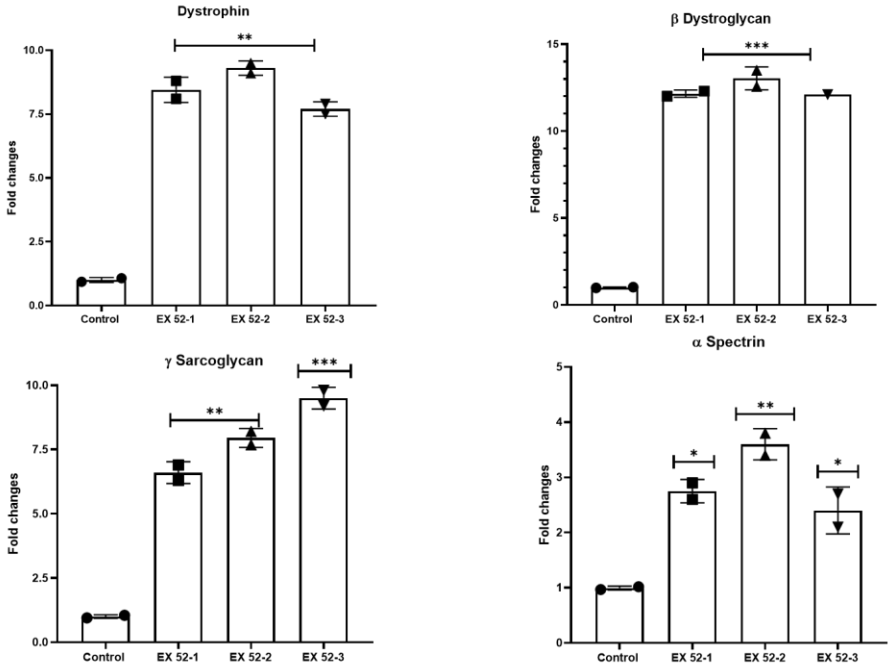

Figure 2. Comparison of dystrophin, β-dystroglycan, γ-sarcoglycan, and α-spectrin levels in the Control, EX52-1, EX52-2, and EX52-3 groups. Results are expressed as fold change. Dystrophin levels in the experimental groups were statistically significantly higher than in the control group. β-dystroglycan expression was also significantly increased relative to the control. γ-sarcoglycan levels were significantly elevated in the EX52-1 and EX52-2 groups, with the greatest effect observed in the EX52-3 group. For α-spectrin, an increase was observed in the EX52-2 group, whereas the EX52-3 and EX52-1 groups showed a lower increase than EX52-2 (*$p < 0.05$, **$p < 0.01$, ***$p < 0.001$).

3.1.2. Immunohistochemistry Analysis for Muscles

The pathological examination results are shown in Figure 3. The data obtained indicate that all treatment groups showed significantly higher dystrophin levels than the control group. The increase rate was determined to be 18.96% in EX 52-1 and EX-52-2, and 26% in EX 52-3.

 doi:10.20944/preprints202511.0016.v2

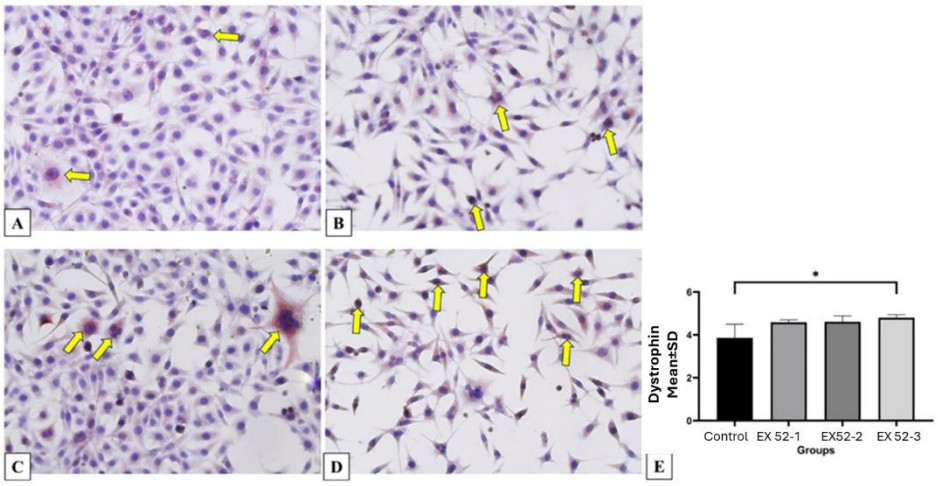

Figure 3. Staining of functional dystrophin structure. Brown indicates dystrophin expression. Increased brown staining was observed in the experimental groups compared to the control group, and the optical density (OD) values support this observation. (A) Control group, (B) EX52-1 group, (C) EX52-2 group, and (D) EX52-3 group. (E) OD values of dystrophin structure (*$p < 0.05$).

Synthesis of dystrophin protein alone is not a sufficient criterion for the treatment of Duchenne muscular dystrophy. The produced protein must have the correct three-dimensional conformation, effectively localize to the cell membrane (sarcolemma), and perform its biological function by interacting with dystrophin-associated protein complexes. Therefore, in addition to quantitatively demonstrating protein expressions, evaluating its structural and functional integrity at the cellular level is critically important. For this reason, the method's effectiveness was first validated by analyzing dystrophin expression and localization in in vitro cell culture models. These preliminary data, obtained from in vitro experiments, demonstrated the reliability of the experimental approach and provided the basis for planning in vivo experiments to validate it in more complex biological systems. Accordingly, guided by in vitro findings, an in vivo experimental design was created to comprehensively evaluate the tissue-level expression, membrane localization, and functional effects of dystrophin.

3.2. In Vivo Test for EXON 52, 51, 48, and 47 mRNA Complex

Based on findings from in vitro analyses, in vivo studies targeting exons 47, 48, 51, and 52 were conducted using mRNA sequences with the highest efficacy for protein and gene expression. These studies were conducted in mdx/D2 mouse models that reflect the pathophysiology of Duchenne Muscular Dystrophy (DMD).

Molecular, Western blot, IHC, and IF analyses were performed on muscle tissues isolated from experimental animals after mRNA treatments targeting exons 47, 48, 51, and 52 were applied. The results showed increased target gene and protein expression across all treatment groups compared with the control group. Particularly in the groups treated with exon 47- and exon 52-targeted mRNA, more significant increases were observed in the levels of dystrophin, β-dystroglycan, γ-sarcoglycan, and α-spectrin, which are key components of the dystrophin-associated protein complex.

Significant improvements were also observed in exon 48 and 51 groups, although these increases were more limited compared to exon 47 and 52 groups. Overall, in vivo findings, consistent with in vitro data, revealed that mRNA therapies targeting specific exons can increase functional protein expression in muscle tissue. These results support the idea that the developed mRNA-based approach could be a potential treatment strategy for DMD.

 doi:10.20944/preprints202511.0016.v2

3.2.1. Behavioral Analyses

Rotarod and motor function test results are shown in Figures 4A and 4B. The results showed a significant decrease in resting time across all groups compared with the DMD control group ($P < 0.01$). The rotarod test results are shown in Figure 4A. When the results were evaluated, the DMD control group had very short rotarod latency during the 200-second test period and exhibited a high number of falls. In contrast, a significant decrease in the number of falls and an increase in time spent on the rotarod were observed across all groups treated with mRNA-based therapy ($P<0.01$).

The results of the motor activity test are shown in Figure 5B. The results indicate that motor activity is significantly reduced in the DMD control group. The impairment in motor function is like that observed in patients with DMD. In contrast, a significant increase in motor activity levels was observed in all groups treated with mRNA-based therapy. However, the EX52 group exhibited higher motor activity. Similarly, motor activity was significantly increased in the EX47 and EX51 groups.

In conclusion, our findings show that treatment with an mRNA complex increases rotarod performance and motor activity in D2.mdx mice, thereby improving muscle function ($P<0.01$).

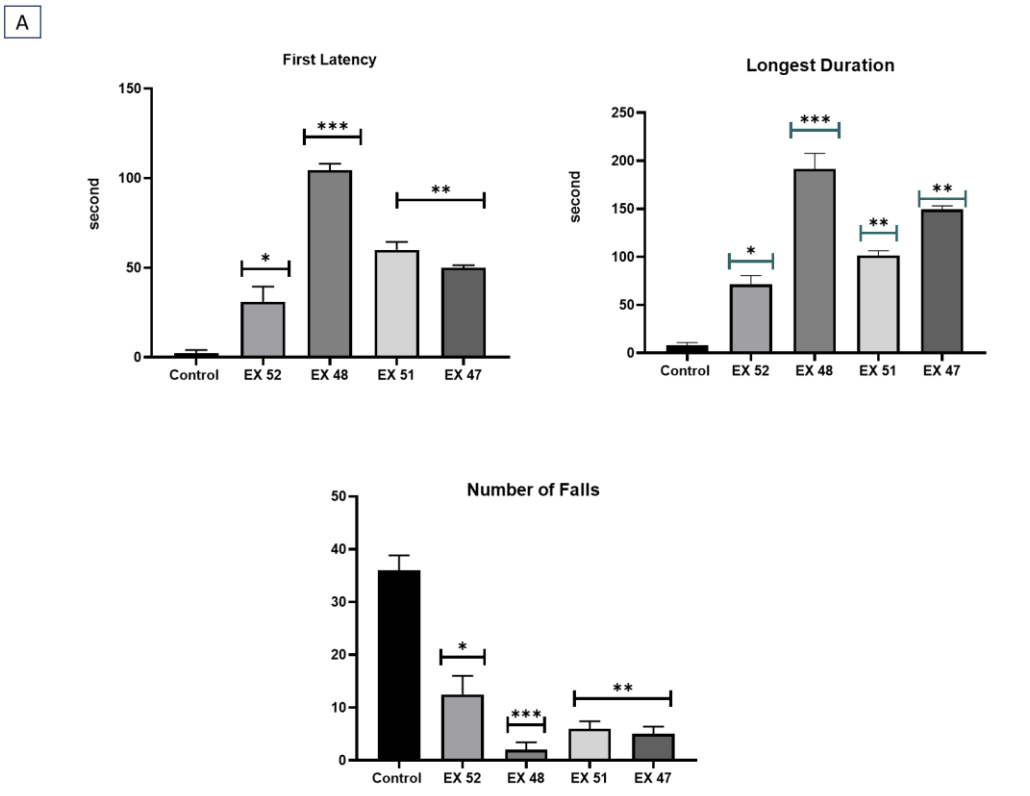

 doi:10.20944/preprints202511.0016.v2

Figure 4. Behavioral test results of mdx/d2 mouse groups (n=8). (A) The EX52 group showed a significantly longer latency to fall than the control group. The EX51 and EX47 groups maintained their positions longer than the EX52 group, with the highest endurance in the EX48 group. The number of falls decreased in EX52 compared with control, and further in EX51 and EX47, with the lowest in EX48. (B) Total distance moved increased in EX48 versus control; EX51 and EX47 moved farther, and the highest distance was in EX52. Immobility duration was shortest in EX52, followed by EX51 and EX47, and EX48 versus control (*$p < 0.05$, **$p < 0.01$, ***$p < 0.001$).

3.2.2. ELISA Analyses

In DMD pathology, increased oxidative stress and chronic inflammation are key determinants of progressive muscle damage and functional loss. Klotho and PPARγ, which regulate these processes, are critically important for cellular protective mechanisms. The premature aging phenotypes exhibited by Klotho-deficient mice, such as shortened lifespan, sarcopenia, severe muscle wasting, hypokinesia, abnormal gait, decreased stride length, muscle weakness, and reduced running endurance, clearly demonstrate the crucial role of this protein in maintaining muscle integrity and physical function. The increase in Klotho and PPARγ levels observed in this study, along with the suppression of oxidative stress and inflammation, suggests a potential therapeutic effect in preserving muscle function in DMD.

Figure 5A presents data from the Total Oxidative Status (TOS) test, expressed in H_2O_2 equivalents/L^{-1}. The DMD control group showed a TOS level of 4.9 H_2O_2 Equiv/L^{-1}. All treated groups exhibited lower TOS levels than the control. The TOS values for the EX52, EX51, and EX47 groups were similar to one another and significantly lower than those of the DMD control group ($P<0.01$). While the EX48 group also showed a decrease in TOS, it was less pronounced and less statistically significant ($P<0.05$).

Analysis of nitric oxide (NO) levels revealed that they were low (1.8 nM) in the DMD control group. Significant increases in NO levels were observed in the treated groups. In groups EX51, EX52, and EX47, NO levels were statistically significantly higher than in the DMD control group ($P<0.01$). In contrast, the significance level for NO levels was lower in group EX48 than in the other groups ($P<0.05$).

These findings demonstrate that most treatments can restore nitric oxide bioavailability, which is impaired in DMD pathology, and that they can positively affect vascular function and cellular signaling.

Data on α-Klotho and PPARγ protein levels are presented in Figure 5, with results expressed in nM. In the DMD control group, α-Klotho was measured at 2.4 nM. An increase in α-Klotho levels was observed across all treated groups ($P<0.05$), with the increase significantly more pronounced in EX52, EX51, and EX47 than in the DMD control group ($P<0.01$).

The PPARγ level was 1.4 nM in the DMD control group. PPARγ levels were significantly increased in groups EX52, EX51, and EX47 compared to the control group ($P<0.05$). In contrast, no statistically significant difference was found in PPARγ levels between group EX48 and the other groups ($P>0.05$).

Overall, the findings suggest that reducing oxidative stress and inflammation, while increasing Klotho and PPARγ levels, provides comprehensive protection in DMD. This approach helps maintain muscle cell structure, enhances metabolic balance, and limits declines in muscle function.

 doi:10.20944/preprints202511.0016.v2

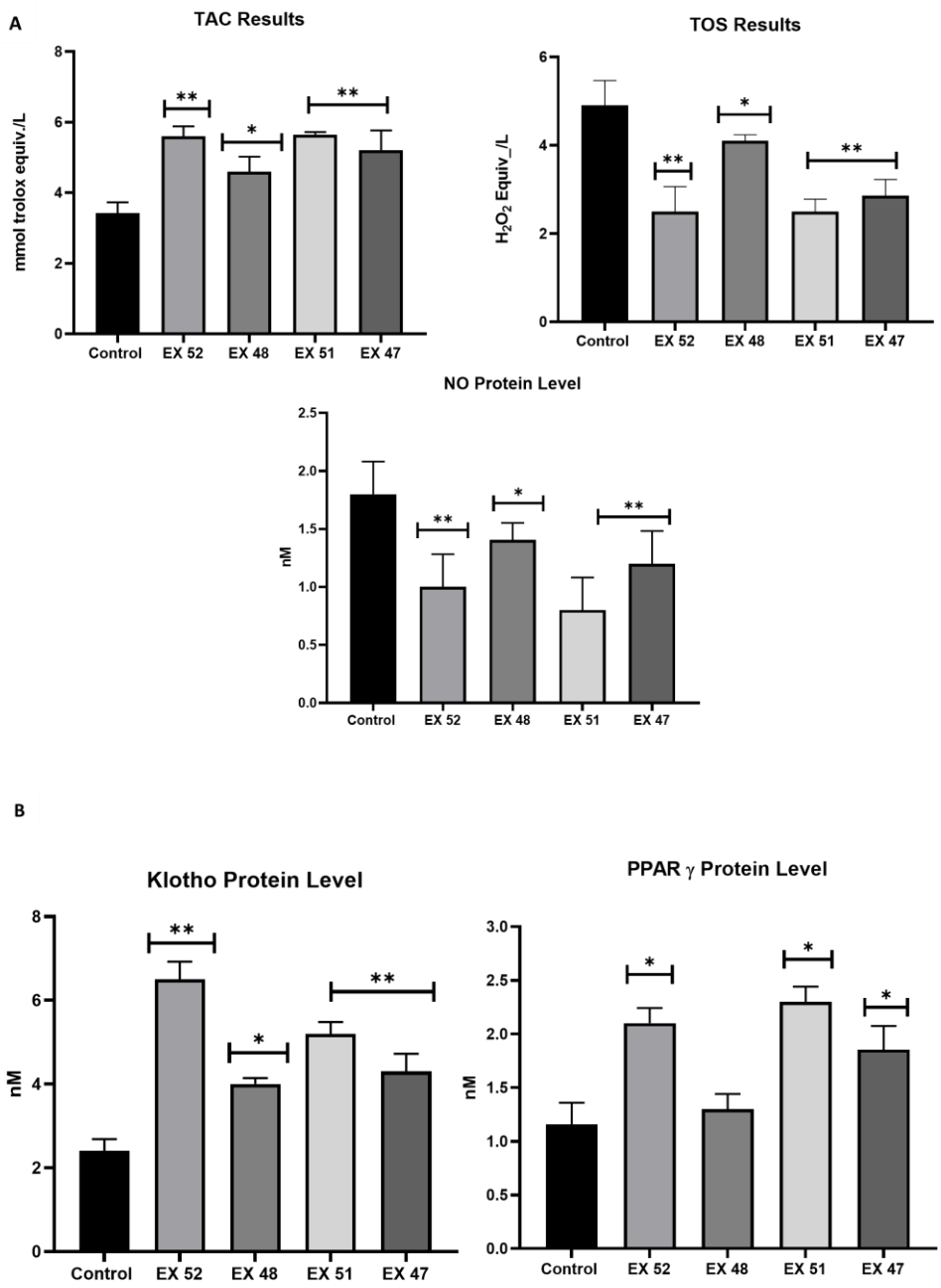

Figure 5. TAC, TOS, NO, Klotho, and PPARγ levels in muscle tissues obtained from mdx/d2 mice. **(A)** TAC, TOS, and NO protein levels in the EX-52, EX-48, EX-51, and EX-47 groups were compared with those of the control group. **(B)** Klotho and PPARγ protein levels in the EX-52, EX-48, EX-51, and EX-47 groups were compared with those of the control group. **(A)** TAC levels were significantly increased in the EX-48 group compared to the control group. Higher TAC values were observed in the EX-52, EX-51, and EX-47 groups relative to the EX-48 group. Regarding TOS results, a significant decrease was detected in the EX-48 group compared to the control group. Significantly lower TOS levels were observed in the EX52, EX51, and EX-47 groups compared to the EX-48 group. NO protein levels were significantly reduced in the EX48 group compared to the control group. In the EX-52, EX-51, and EX-47 groups, NO levels remained lower than those in the EX-48 group, showing a significant decrease. **(B)** Klotho protein levels were markedly and significantly increased in the EX-48 group compared to the control group, and significant differences in Klotho levels were also observed among the EX-52, EX-51, and EX-47 groups. PPARγ protein levels were significantly increased in the EX-52 group compared to the control group. In addition, higher PPARγ levels were measured in the EX-51 group compared to the EX-48 group (*$p < 0.05$, **$p < 0.01$).

 doi:10.20944/preprints202511.0016.v2

3.2.3. Gene Expression Analyses

The expression levels of dystrophin, β-Dystroglycan, γ-sarcoglycan, α-Spectrin, IL-1, IL-6, IL-8, and IL-10 are shown in Figure 6. The DMD control group was assigned a 1-fold ratio. The data indicate that expression levels of dystrophin, β-Dystroglycan, γ-sarcoglycan, and α-Spectrin were significantly higher in all treatment groups. Based on IL markers, inflammation was reduced. β-Dystroglycan levels were nearly 15 times higher in the EX5-1 group, while the lowest was 2.5 times in the EX-48 group ($P<0.01$). In γ-Sarcoglycan levels, expression was nearly 9-fold higher in the EX-51 and EX-47 groups ($P<0.01$), while the lowest was 1.8-fold in the EX-48 group ($P<0.05$). In α-Actin levels, expression was nearly 8 times higher in the EX-52 and EX-51 groups ($P<0.01$), while the lowest was 1.6 times in the EX-48 group ($P<0.05$).

IL-1 expression decreased in all groups except EX-48. The most significant decrease, nearly 0.6-fold, was observed in the EX-47 and EX-51 groups ($P<0.01$). The EX-48 group showed a 1.2-fold decrease ($P<0.05$). IL-6 expression levels decreased across all treatment groups except EX-48. The most notable reductions were observed in the EX-52 and EX-47 groups, with approximately 0.6-fold decreases ($P<0.01$). The EX-48 group showed a 1.4-fold decrease ($P<0.05$). IL-8 expression levels decreased in all treatment groups except EX48. The most notable reduction was observed in the EX-52 and EX-51 groups, approximately 0.4-fold ($P<0.05$). There was no significant difference between the EX-48 and EX-51 groups ($P>0.05$). IL-10 expression levels decreased in all treatment groups except EX-48. The most significant increase was observed in the EX-51 and EX-52 groups, approximately 3-fold ($P<0.01$). There was no significant difference in the EX-48 group ($P>0.05$).

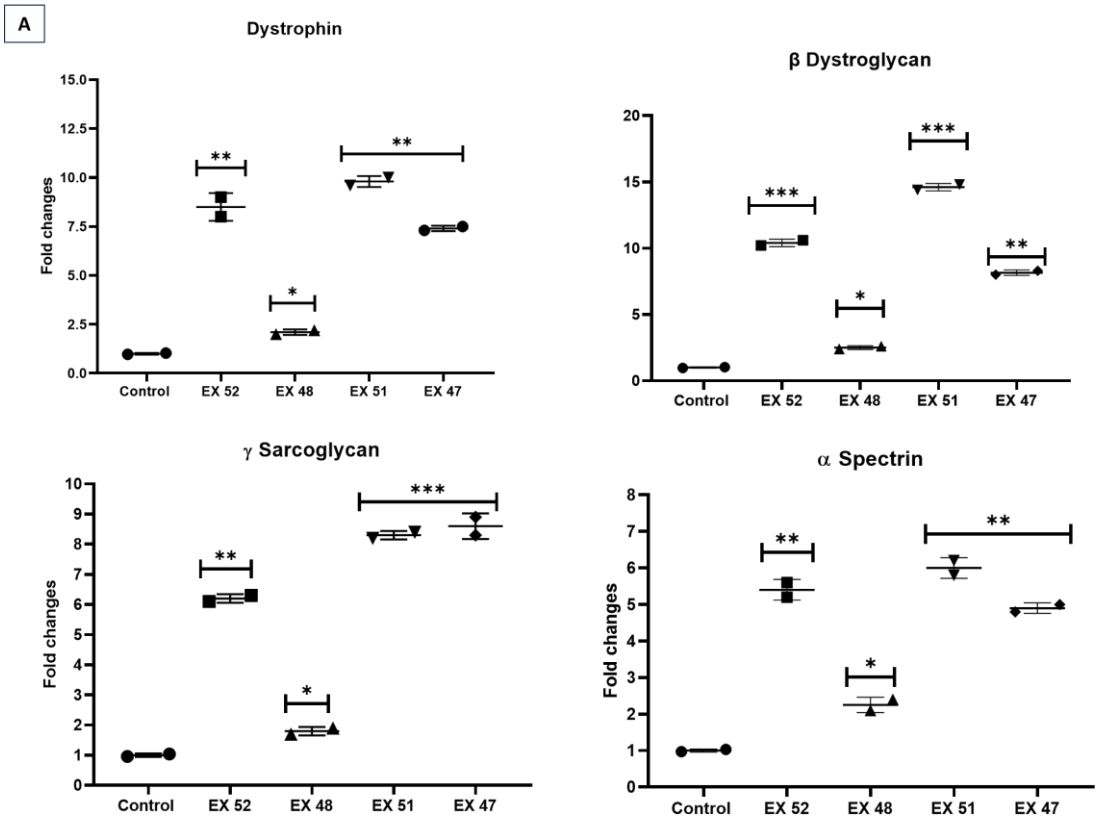

 doi:10.20944/preprints202511.0016.v2

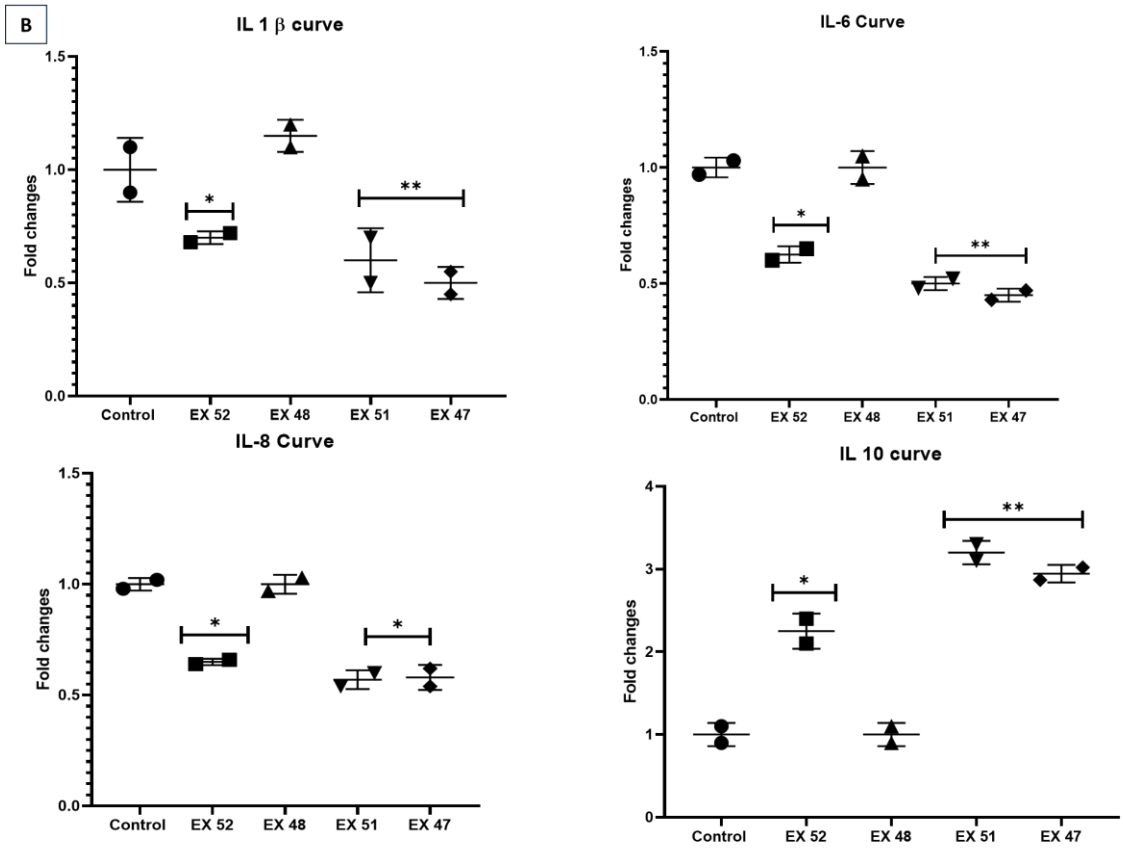

Figure 6. Muscle tissue obtained from mdx/d2 mice and dystrophin, β-Dystroglycan, γ-sarcoglycan, α-Spectrin, IL-1, IL-6, IL-8, and IL-10 expression levels. **(A)** Dystrophin levels were significantly increased in the EX-48 group compared to the control group, while marked increases were observed in the EX-52 and EX-51 groups. β-dystroglycan expression was significantly elevated in the EX-48 group relative to the control group, with a continued significant increase in the EX-47 group. The highest levels were detected in the EX-52 and EX-51 groups. γ-sarcoglycan levels were significantly increased in the EX-48 group compared to the control group. Relatively higher values were observed in the EX-52 group compared to EX-48, while the highest expression levels were reached in the EX-51 and EX-47 groups. α-spectrin levels were significantly elevated in the EX-48 group compared to the control group; values were further increased in the EX-52 and EX-47 groups relative to EX-48, with the greatest increase observed in the EX-51 group. **(B)** IL-1β and IL-6 levels were significantly reduced in the EX-52 group compared to the control group, with greater reductions observed in the EX51 and EX-47 groups. No decrease was observed in the EX-48 group. IL-8 levels were significantly decreased in the EX-52, EX-51, and EX-47 groups compared to the control group. The anti-inflammatory cytokine IL-10 level was increased in the EX-52 group relative to the control group, with the highest increase observed in the EX-51 and EX-47 groups compared to the other groups (*$p < 0.05$, **$p < 0.01$, ***$p < 0.001$).

3.2.4. Western Blot Analyses

Western blot analysis revealed differential expressions of dystrophin, β-dystroglycan, and γ-sarcoglycan among mdx/d2 mouse groups. Compared to the control group, the EX52 group showed a significant increase in dystrophin, β-dystroglycan, and γ-sarcoglycan levels. Furthermore, expression levels in the EX-48 β-dystroglycan and γ-sarcoglycan family were observed to be quite close to those of EX-52. No significant difference was detected in EX-51 and EX-47 compared to the control group. β-actin was used as a loading control to confirm equal protein loading across all samples. These results demonstrate a gradual increase in dystrophin, β-dystroglycan, and γ-sarcoglycan expression associated with treatment intensity or group definition.

 doi:10.20944/preprints202511.0016.v2

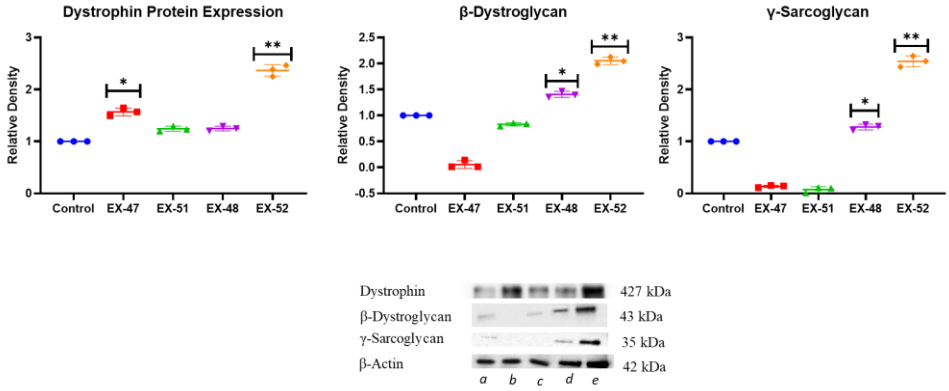

Figure 7. Expression levels of EX-47, EX-51, EX-48, and EX-52 proteins were modulated by Western blot analysis (Mean ± SD and n = 3). Protein bands of dystrophin, β-dystroglycan, and γ-sarcoglycan expression levels were used as β-actin loading control proteins (a; Control, b; EX-47, c; EX-51, d; EX-48, e; EX-52) (* $p < 0.05$, ** $p < 0.01$).

3.2.4. Immunofluorescence and Immunohistochemistry Analysis for Muscles

Histopathological examination revealed myofibrils of unequal size in the control group, generally round in diameter, and with increased centrally located nuclei. Inflammatory cell infiltration and areas of necrotic tissue were observed. It was determined that these histopathological findings were also observed in the other EX-52, EX-48, EX-51, and EX-47, but decreased from EX-52 to EX-47 (Figures 8,9 and 10).

Cont: When muscle and heart tissues were examined histopathologically, severe degeneration and necrosis were observed in muscle fibers and myocytes in the heart muscle, gluteal muscles, and tongue muscle, along with inflammation and edema in the interstitial spaces and mild fat accumulation (Figures 8-9).

EX-52: When muscle and heart tissues were examined histopathologically, moderate degeneration and necrosis were determined in muscle fibers in the heart muscle, gluteal muscles, and tongue muscle, along with inflammation in the interstitial spaces (Figures 8-9).

EX-48: When muscle and heart tissues were examined histopathologically, mild degeneration and necrosis were detected in muscle fibers in the heart muscle, gluteal muscles, and tongue muscle (Figures 8-9).

EX-51: Histopathological examination of muscle and heart tissues revealed mild inflammation and edema in the interstitial spaces of muscle fibers in the heart muscle, gluteal muscles, and tongue muscle (Figures 8-9).

EX-47: Histopathological examination of muscle and heart tissues revealed mild inflammation and edema in the interstitial spaces of muscle fibers in the heart muscle, gluteal muscles, and tongue muscle (Figures 8-9).

Histopathological examination of the brain, kidney, and intestinal tissues revealed no statistically significant difference in pathological findings (Figure 10).

Immunofluorescence analysis showed no pathological findings in the brain, kidney, or intestinal tissues (Figures 11-15).

DMD Control: When muscle and heart tissues were examined using immunofluorescence, very mild intracytoplasmic expression of α-Spectrin, β-dystroglycan, α-actin, and γ-sarcoglycan was observed in the muscle fibers of myocytes.

EX-52: When muscle and heart tissues were examined using immunofluorescence, moderate intracytoplasmic expression of α-Spectrin, β-dystroglycan, α-actin, and γ-sarcoglycan was observed in the muscle fibers of myocytes.

EX-48: When muscle and heart tissues were examined using immunofluorescence, moderate intracytoplasmic expression of α-Spectrin, β-dystroglycan, α-actin, and γ-sarcoglycan was observed in the muscle fibers of myocytes.

 doi:10.20944/preprints202511.0016.v2

EX-51: When muscle and heart tissues were examined using immunofluorescence, significant intracytoplasmic expression of α-Spectrin, β-dystroglycan, α-actin, and γ-sarcoglycan was observed in myocyte muscle fibers.

EX-47: When muscle and heart tissues were examined using immunofluorescence, significant intracytoplasmic expression of α-Spectrin, β-dystroglycan, α-actin, and γ-sarcoglycan was observed in the muscle fibers of myocytes. Statistical data for the immunofluorescence results are shown in Figure 14.

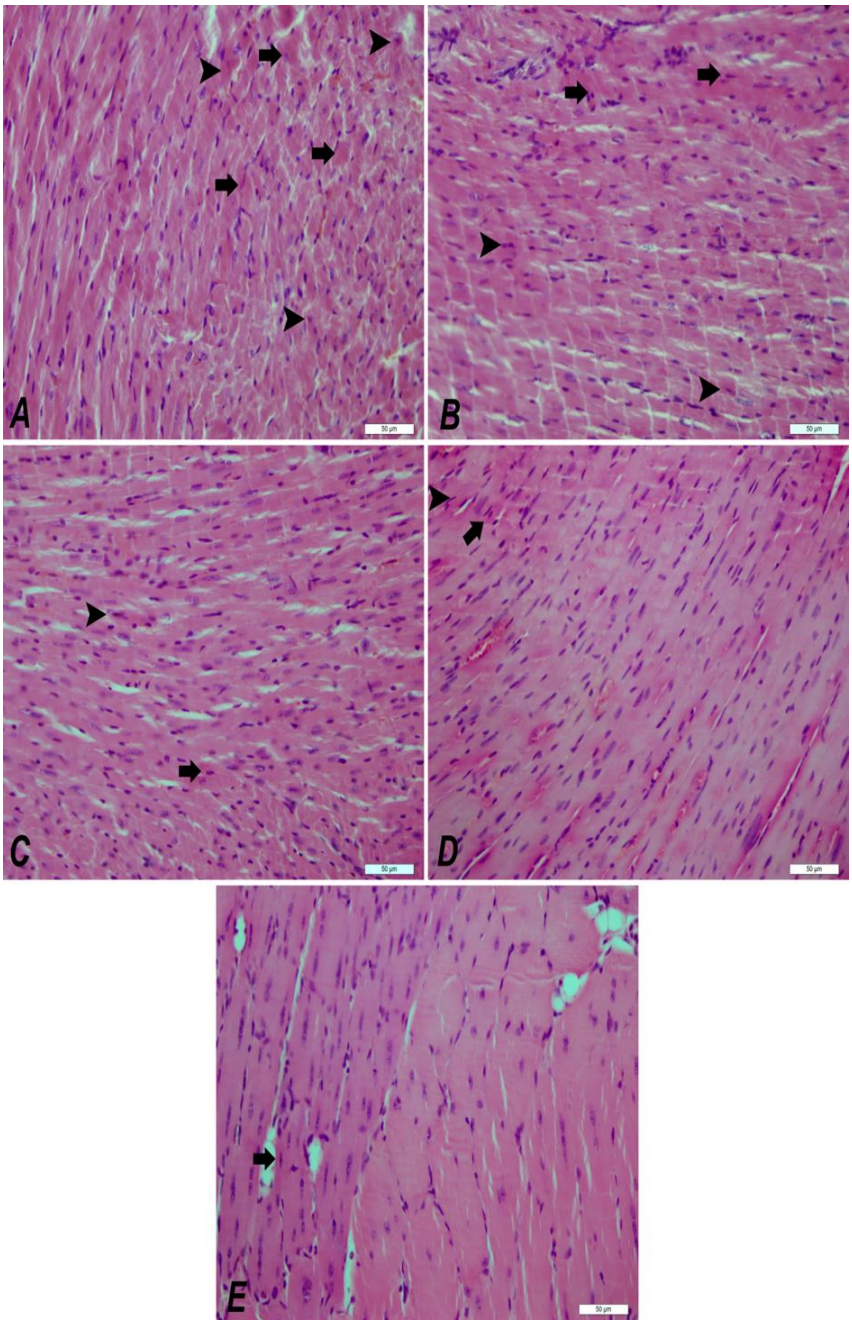

Figure 8. Hematoxylin and eosin staining of cardiac muscle tissue from mdx/d2 mice. Degeneration and necrosis in DMD Control (A), EX-52 (B), EX-48 (C), EX-51 (D), EX-47 (E) myocytes, inflammation in interstitial spaces, H&E, Bar: 50µm. Degeneration (arrows) and necrosis (arrowheads) in myocytes.

 doi:10.20944/preprints202511.0016.v2

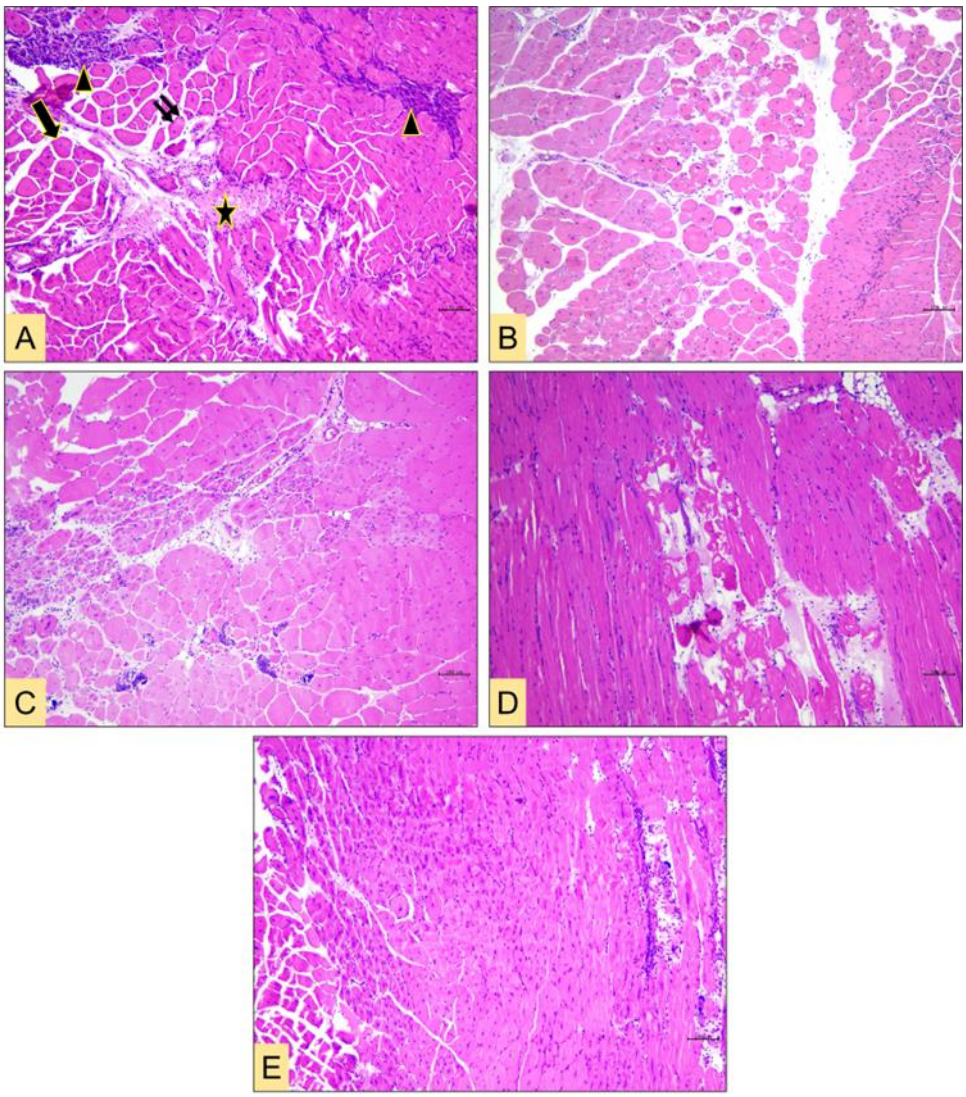

Figure 9. Hematoxylin and eosin staining of muscle tissue from mdx/d2 mice. DMD Control (A), EX-52 (B), EX-48 (C), EX-51 (D), EX-47 (E) myocyte degeneration and necrosis, inflammation in interstitial spaces, H&E, Bar: 100μm. Although the pathological findings in the control group were observed across all groups, they decreased from EX-52 to EX-47. The pathological findings are as follows: Arrowhead: inflammatory cell infiltration, Single Arrow: round myofibril, Double Arrow: myofibril with a centrally located nucleus, and Star: necrotic areas. The bars in all shapes are 100 μm.

 doi:10.20944/preprints202511.0016.v2

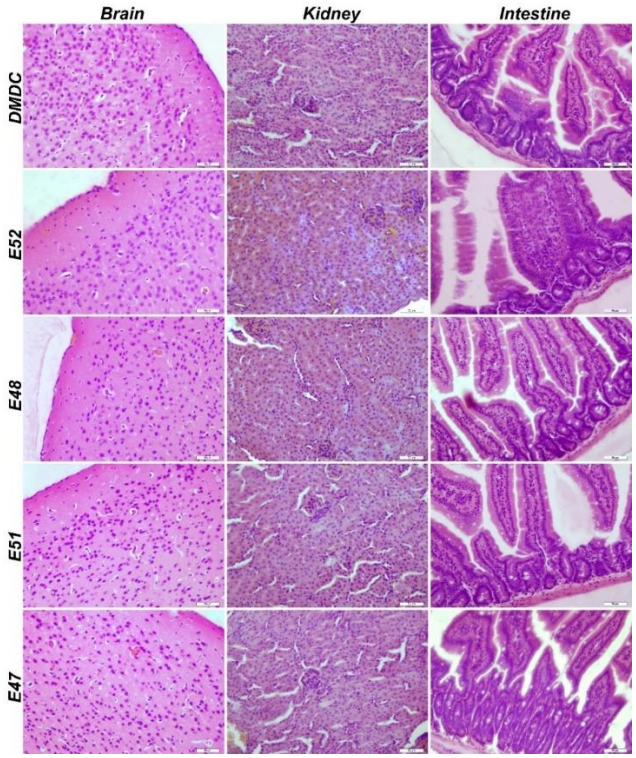

Figure 10. Hematoxylin and eosin staining of brain, kidney, and intestinal tissues of mdx/d2 mice (Control, H&E, Bar: 50μm). This section may be divided by subheadings. It should provide a concise, precise description of the experimental results, their interpretation, and the conclusions that can be drawn.

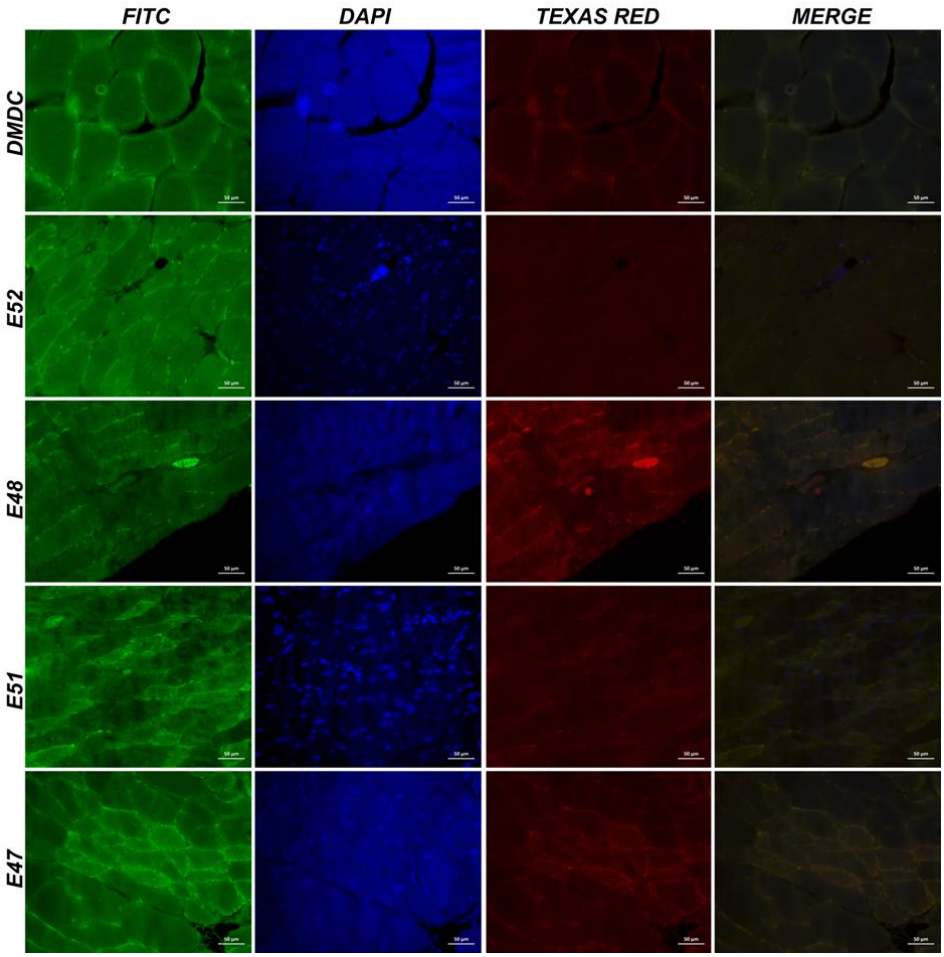

 doi:10.20944/preprints202511.0016.v2

Figure 11. IF images of cardiac muscle tissue obtained from mdx/d2 mice (Intracytoplasmic α-Spectrin expressions (FITC) and α-actin expressions (Texas Red) in myocytes, IF, Bar: 50µm).

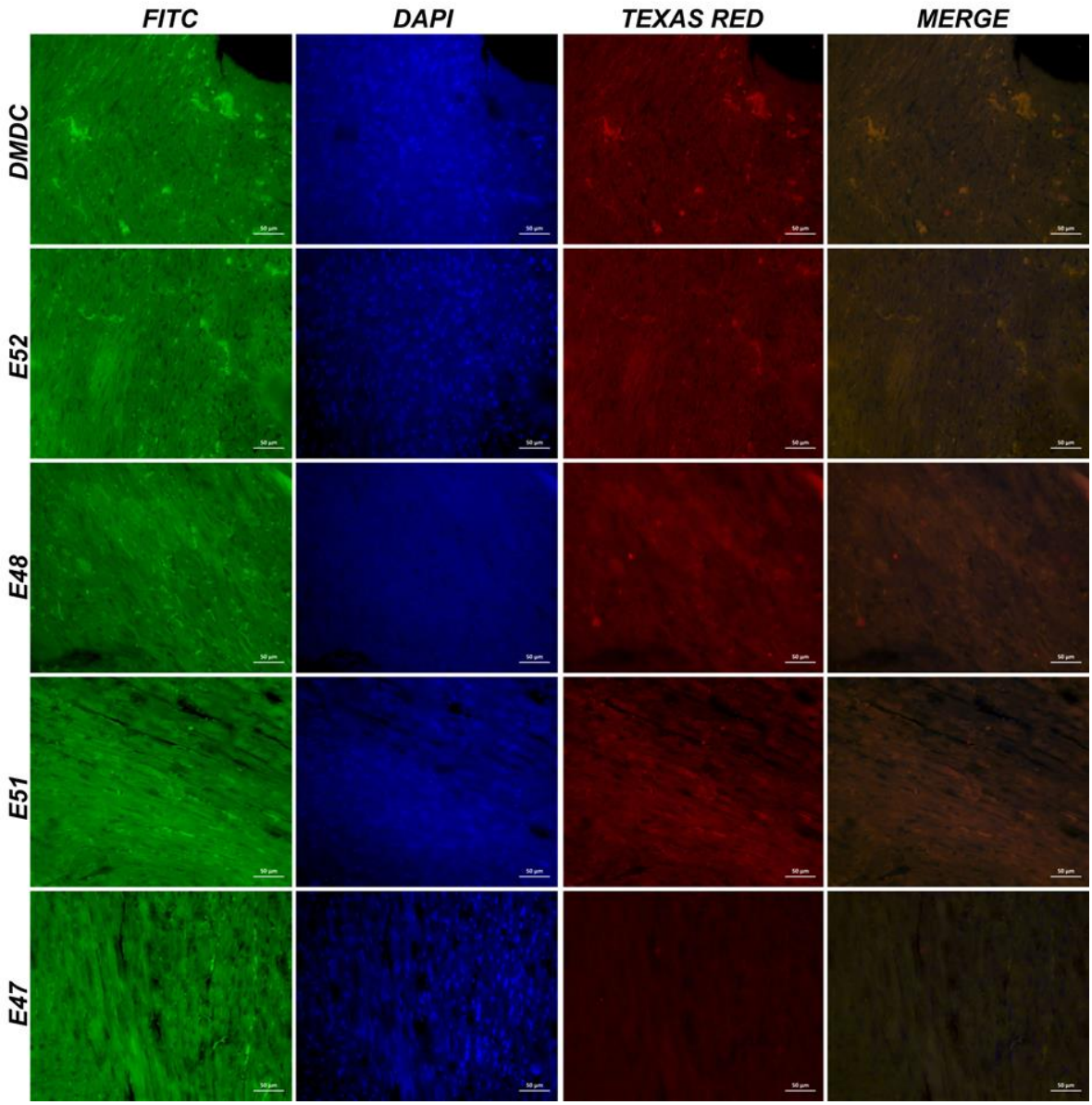

Figure 12. IF images of muscle tissue obtained from mdx/d2 mice (Intracytoplasmic Spectrin α expressions (FITC) and α-actin expressions (Texas Red) in myocytes, IF, B.

 doi:10.20944/preprints202511.0016.v2

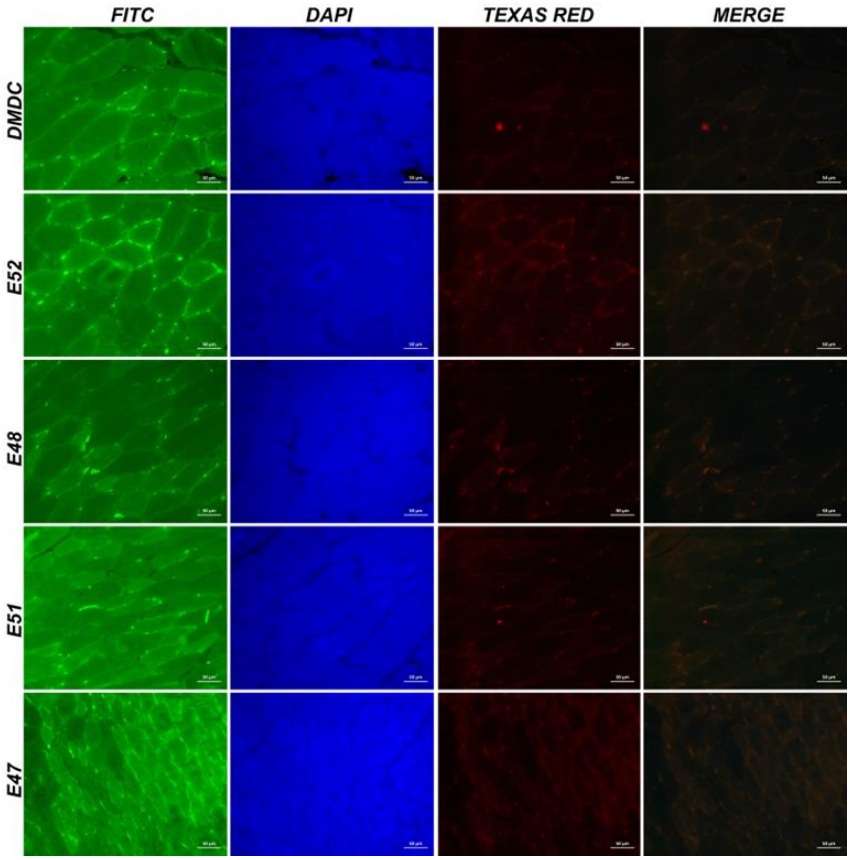

Figure 13. IF images of cardiac muscle tissue obtained from mdx/d2 mice (Intracytoplasmic β-dystroglycan expressions (FITC) and γ-sarcoglycan expressions (Texas Red) in myocytes, IF, Bar: 50μm).

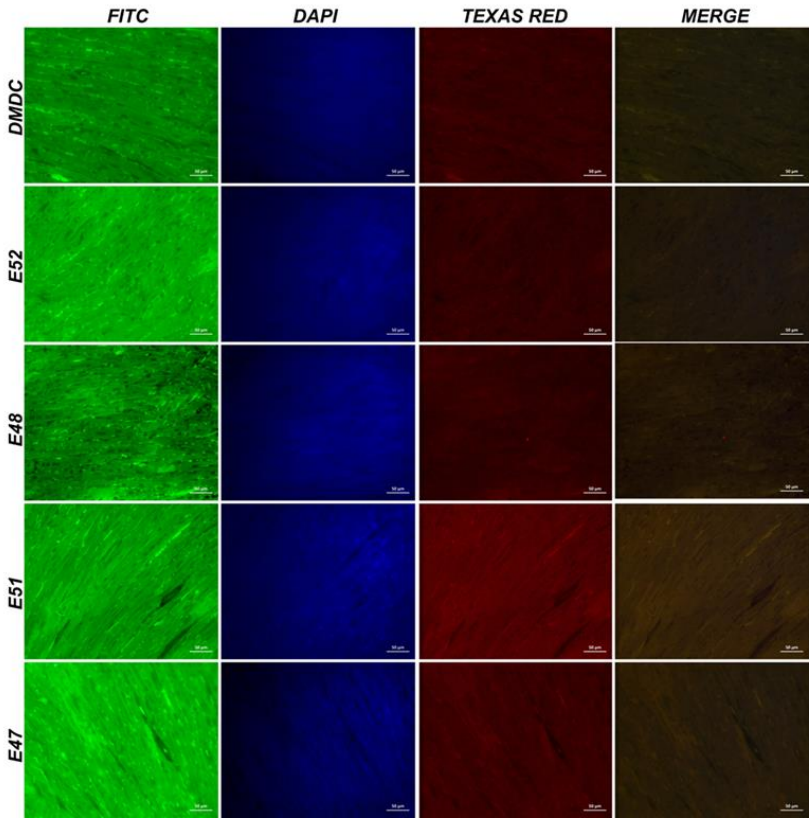

Figure 14. IF image of muscle tissue obtained from mdx/d2 mice (Intracytoplasmic β-dystroglycan expressions (FITC) and γ-sarcoglycan expressions (Texas Red) in myocytes, IF, Bar: 50μm).

 doi:10.20944/preprints202511.0016.v2

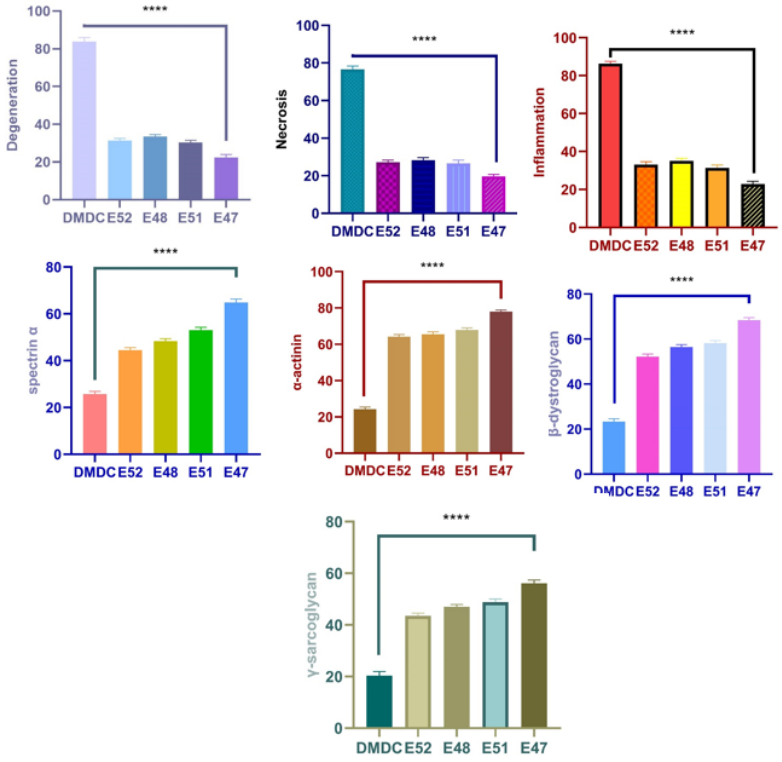

Figure 15. Statistical analysis of histopathological findings and immunofluorescence staining results seen in muscle tissue. Myocyte degeneration (****P<0.0001), myocyte necrosis (****P<0.0001), inflammation (****P<0.0001), α-Spectrin expression levels (****P<0.0001), α-actin expression levels (****P<0.0001), and β-dystroglycan expression levels (****P<0.0001), γ-sarcoglycan expression levels (****P<0.0001).

Immunohistochemistry was used to evaluate the expression of dystrophin, α-Ssectrin, β-dystroglycan, and γ-sarcoglycan in striated muscle tissue of the groups. Dystrophin expression was increased in the EX-51 (13.6±3.8%) and EX-47 (8.63±3.06%) groups compared to the control group (1.24±0.09%) ($p<0.05$). Expression in the EX-48 group (2.52±0.65%) was lower than in the EX-51 and EX-47groups ($p<0.05$). There was no significant difference in dystrophin optical density between the EX-52 (4.49±1.63%) and control groups ($p>0.05$). α-Spectrin immunoreactivity was found to be low in all groups and, although it showed an increasing trend from control to EX-47, it did not show a statistically significant difference (Control 0.03±0.01%, EX-52 0.05±0.04%, EX-48 0.11±0.04%, EX-51 0.27±0.1%, EX-47 0.28±0.14%) ($p>0.05$) (Figure 16).

When we examined β-dystroglycan immunoreactivity between the groups, no reaction was observed in the control group. The percentage optical densities in the groups were as follows: EX-52: 10.19±0.81; EX-48: 2.71±1.01; EX-51: 9.97±2.55; and EX-47: 5.24±1.38. No statistically significant difference in β-dystroglycan immunoreactivity was observed between the EX-52, EX-48, EX-51, and EX-47 groups ($p>0.05$). No γ-sarcoglycan immunoreactivity was detected in the groups (Figure 16).

 doi:10.20944/preprints202511.0016.v2

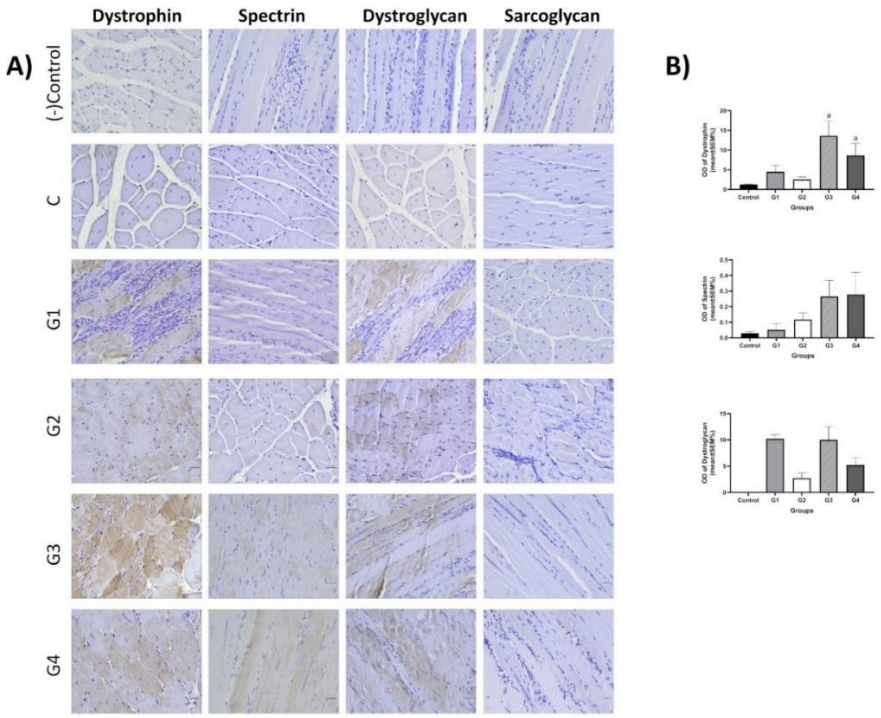

Figure 1. IHC staining of the groups. Groups Control, Control, G1: EX-52, G2: EX-48, G3: EX-51, and G4: EX-47. (A) Representative immunohistochemical images of striated muscle tissue showing dystrophin, α-spectrin, β-dystroglycan, and γ-sarcoglycan expression in the experimental groups. Sarcoglycan immunoreactivity was not detected. Scale bar: 30 μm. (B) Comparison of optical densities among the groups. Kruskal–Wallis test; *a* indicates statistical significance compared with the Control and EX-52 groups ($p < 0.05$).

4. Discussion

Duchenne Muscular Dystrophy (DMD) is a serious neuromuscular disease characterized by progressive muscle degeneration, chronic inflammation, and fibrosis resulting from dystrophin deficiency. The absence of dystrophin disrupts the mechanical stability of the muscle cell membrane, initiating a complex pathological process that results in recurrent damage, necrosis, and the eventual replacement of muscle fibers with fat and fibrotic tissue. Therefore, therapeutic approaches aimed at restoring dystrophin expression are among the key research areas in DMD treatment. In this study, the efficacy of an mRNA-based treatment strategy targeting common exon 47, 48, 51, and 52 deletions in the DMD mutation spectrum was evaluated in both DMD patient-derived primary cells (in vitro) and the mdx/D2 mouse model (in vivo), which more closely reflects the pathophysiology of the human disease. The findings indicate that the designed mRNA complex has the potential to induce dystrophin production, suggesting that mRNA-based approaches could be a promising alternative among the new treatment strategies being developed for DMD.

Behavioral Tests

Motor function tests are routinely used to assess movement ability. An increase in movement ability or a decrease in rest periods indicates that motor cortex and muscle coordination have been achieved [24]. An increase in ambulatory ability is directly related to muscle strength and dystrophin expression. The applied treatment has been found to increase the ability to move and stay on the rotarod during the experiment [25]. Studies have shown improvements in wire-holding time and rotarod walking time in treated mice that produce dystrophin compared to controls [26]. In the DMD control group, due to decreased muscle strength (along with increased fatigue), mdx/d2 mice frequently fall from the rotating plate. Visible improvement in muscle strength was observed in the

 doi:10.20944/preprints202511.0016.v2

EX48 group, with an average drop of 8 times (control group: 34 times), indicating that the dystrophin produced is functional.

The motor test is similar to the rotarod test. Studies have shown that the experimental mice traveled a shorter distance than the control group. However, the treated mice were found to move more vigorously and walk longer distances [27].

Determining Gene Expression Levels

Dystrophin forms the internal link with α-actin, while β-dystroglycan, γ-sarcoglycan, and α-spectrin connect to the extracellular matrix. Therefore, investigating this complex in its entirety is essential to assessing the study's success. CRISPR-Cas9, one of the leading methods currently used to treat DMD, increases dystrophin levels. However, it is emphasized that fibrosis negatively affects muscle development. Therefore, they suggest a gradual improvement in the treatment processes described [28]. Studies have reported increases in dystrophin production after treatment ranging from 6.255 to 11% [29]. The exact amount of dystrophin sufficient for DMD patients is unknown.

In DMD patients with mutations amenable to exon 51 skipping, this treatment increased dystrophin expression by 0.28% and 0.93% at 48 and 180 weeks, respectively [30]. A significant difference was demonstrated in the 6-minute walk test 36 months after initial treatment. A phase 3 study demonstrated that monthly dosing of SRP-5051, with exon 51 skipping, at 30 mg/kg resulted in an average increase in dystrophin expression of 6.55% in patients with DMD [28].

In the study by Paola et al., ROS-activated tyrosine kinase in DMD promotes the degradation of β-dystroglycan (β-DG), a component of the dystrophin-glycoprotein complex that can amplify damaging signals. In mdx/d2 mice, a 4-week subcutaneous treatment with dasatinib (DAS), a pan-Src-TKs inhibitor approved as an anti-leukemic agent, increased muscle β-DG and resulted in minimal improvements in morphofunctional indices. The study is valuable because it conducted a single β-dystroglycan trial in a DMD model [31]. In our research, TAC, MTT, TOS, IL-1-6-8-10, and β-dystroglycan ratio were evaluated. TAC and TOS, which correspond to ROS parameters, showed that muscle inflammation and oxidative stress decreased after our treatment. Survival rates were higher in the treatment groups than in the DMD control group. Additionally, the expression level of the β-dystroglycan gene increased nearly 15-fold in the EX51 group, suggesting that β-, γ-, and δ-sarcoglycan function as a single unit. Notably, myofiber degeneration can occur independently of dystrophin in γ-sarcoglycan-deficient mice, even though they have normal dystrophin levels and localization. Furthermore, apoptotic myonuclei are highly expressed in γ-sarcoglycan-deficient skeletal muscles, suggesting that programmed cell death contributes to myofiber degeneration [32]. We showed that γ-sarcoglycan expression increased nearly ninefold in the EX-51 group compared to the DMD control group.

Limited studies in the literature suggest that defects in β-actin and α-spectrin binding sites may occur in dystrophin-deficient muscle [33]. It is known that this error is caused by the degradation of accumulated proteins by proteinases. However, it is normal for the levels of these proteins to increase as reinforcement occurs after bridges form and dystrophins are restored. An eightfold increase in ɒ-actin expression and a nearly sixfold increase in α-spectrin expression were detected in the EX-51 and EX-52 groups.

One study investigated epigenetic silencing of the klotho gene in the mdx mouse model of DMD to determine whether klotho silencing is a key feature of the disease. The data indicated that klotho undergoes muscle-specific silencing during the acute onset of mdx/d2 pathology. Expression of a klotho transgene in mdx/d2 mice has been shown to restore longevity, reduce muscle wasting, improve cellular function, and significantly increase the muscle-resident stem cell pool required for regeneration. Transgene expression was paralleled by decreased fibrosis and reduced expression of collagen types 1 and 3 in the late, progressive stages of mdx/d2 pathology. Therefore, epigenetic silencing of klotho during muscular dystrophy has been suggested to significantly contribute to the loss of regenerative capacity and increased fibrosis of dystrophic muscle in the later stages of DMD [34–36]. In our study, α-Klotho levels were increased in all groups except EX-48 (P>0.05). Data

 doi:10.20944/preprints202511.0016.v2

obtained from groups EX-52, EX-51, and EX-47 showed significant differences compared to the DMD control group ($P<0.01$). Peroxisome proliferator-activated receptor γ (PPARγ) is a transcriptional coactivator that binds to various transcription factors. PPARγ coactivator 1 (PGC-1) has a wide range of biological effects in different tissues [37]. It plays a key role in regulating oxidative metabolism, thereby regulating reactive oxygen species production, autophagy, and mitochondrial biogenesis. Based on these findings, numerous studies aimed at determining the role of PGC-1 in the neuromuscular system have suggested that PGC-1 may be a promising target for treating neuromuscular diseases [38,39]. The restoration of dystrophin and β-dystroglycan, along with increased expression of PPARγ, a key component of cell metabolism, indicates improved function. In our study, PPARγ levels were increased in all groups except EX-48 ($P>0.05$). Data from the EX-52 and EX-51 groups showed a significant difference from the DMD control group ($P<0.05$). The same pattern was also observed in the NO level test [40]. Increased NO levels due to oxidative stress led to a positive treatment response, and our study data showed a decrease in its expression.

Histopathological Findings

Different organs were evaluated at this stage. Dystrophin is expressed in muscle, brain, monocytes, fibroblasts, and, to a lesser extent, in other organs [41,42]. However, a deficiency in dystrophin levels affects the entire system. In DMD, the developmental stages, skeletal muscles, brain, immune system, heart, and lungs are primarily affected. In patients with DMD, muscle biopsy characteristically reveals necrotic or degenerative muscle fibers, often observed in clusters. Macrophages and CD^{4+} lymphocytes surround these necrotic fibers [43]. Additionally, small, immature fibers with central nuclei are observed, reflecting muscle regeneration from myoblasts, thereby balancing necrotic and regenerative processes in the early stages of the disease [44]. Subsequently, the muscles' regenerative capacity appears exhausted, and muscle fibers are gradually replaced by connective tissue and fat. Therefore, the symptoms of Duchenne muscular dystrophy are thought to result from an imbalance between muscle fiber necrosis and myoblast regeneration. Necrosis is the primary pathological feature, but animal evidence suggests that regenerative capacity may decline with age. In our study, histopathological examination of the control DMD group revealed myofibrils of varying sizes, generally rounded in cross-section, with centrally located nuclei. Inflammatory cell infiltration and areas of necrotic tissue were observed. These histopathological findings were also observed in the other EX-52, EX-48, EX-51, and EX-47 groups, but they decreased from EX-52 to EX-47. Immunohistochemistry was used to evaluate dystrophin, α-spectrin, β-dystroglycan, and γ-sarcoglycan expression in striated muscle tissue from each group. Dystrophin expression increased in the EX-51 (13.6±3.8%) and EX-47 (8.63±3.06%) groups compared to the control group (1.24±0.09%) ($P<0.05$).

5. Conclusions

In conclusion, this study demonstrates that an mRNA-based therapeutic approach developed for Duchenne Muscular Dystrophy (DMD) has the potential to induce dystrophin production in both DMD patient-derived primary cells (in vitro) and the D2.mdx mouse model (in vivo). In vitro experiments evaluated different sequences and carrier combinations, and constructs with the highest dystrophin expression were selected and subsequently transferred to in vivo studies. This approach, targeting deletions in exons 47, 48, 51, and 52, which are common in the DMD mutation spectrum, revealed that dystrophin synthesis can be restarted in muscle cells. Furthermore, the use of the mdx/D2 mouse model, which more closely reflects human DMD pathophysiology, allowed for a more meaningful translational evaluation of the findings. The results support the idea that mRNA-based therapies are a promising strategy for dystrophin restoration; however, the effects of this approach on muscle function, long-term efficacy, and safety require validation through more comprehensive functional studies.

6. Study of Limitations

 doi:10.20944/preprints202511.0016.v2

Our study of limitations is the absence of a comparison with the wild-type group. Since the analyses were primarily conducted between treated dystrophic models and the untreated DMD group, the lack of a healthy wild-type control restricts the ability to fully evaluate the extent to which the therapeutic intervention restores physiological conditions. Including a wild-type group would have allowed a more comprehensive interpretation of the functional, molecular, and histological improvements observed following treatment.

Furthermore, while the study demonstrated improvements in dystrophin expression and related muscle membrane proteins, the underlying molecular mechanisms contributing to these changes were not investigated in detail. Future studies incorporating deeper mechanistic analyses, broader molecular profiling, and comparisons with healthy controls may provide a more comprehensive understanding of the therapeutic potential of the proposed approach.

Author Contributions: Conceptualization, D.C., S.G., O.C., and A.T.; methodology, D.C., B.A., D.G.F., S.Y., S.B., K.K., E.N., O.C., E.S., M.K., S.G., and A.T.; validation, D.C., and S.G.; investigation, D.C., S.G., O.C., and A.T.; data curation, D.C., B.A., D.G.F., S.Y., S.B., K.K., E.N., O.C., E.S., M.K., S.G., and A.T.; writing D.C., B.A., D.G.F., S.Y., S.B., K.K., E.N., O.C., E.S., M.K., S.G., and A.T.; writing review and editing, D.C., B.A., D.G.F., S.Y., S.B., K.K., E.N., O.C., E.S., M.K., S.G., and A.T.; supervision, A.T. All authors have read and agreed to the published version of the manuscript.

Funding: This research was funded by the project number 22670, Presidency of Turkish Health Institutes (TÜSEB).

Institutional Review Board Statement: In vitro study: Code: 218345, date: 31.10.2023, Bilecik Şeyh Edebali University Ethics Committee; Animal study: Acıbadem Mehmet Ali Aydınlar University Animal Experiments Local Ethics Committee, ACU-HADYEK-2024/51, July 24, 2024.

Informed Consent Statement: Not applicable.

Data Availability Statement: The dataset presented in this study is available from the corresponding author upon reasonable request.

Acknowledgments: Not applicable.

Conflicts of Interest: The authors declare no conflicts of interest.

Abbreviations

The following abbreviations are used in this manuscript:

DGC	Dystrophin-glycoprotein complex
ECM	Extracellular matrix
DMD	Duchenne Muscular Dystrophy
IHC	Immunohistochemical
IF	Immunofluorescence
PPAR- γ	Proliferator-activated receptor γ
EX	Exon
TAC	Total Antioxidant Capacity
TOS	Total Oxidative Stress
NO	Nitric Oxide

References

1. Ervasti, J.M. and K.P. Campbell, A role for the dystrophin-glycoprotein complex as a transmembrane linker between laminin and actin. The Journal of cell biology, 1993. **122**(4): p. 809-823.
2. Constantin, B., *Dystrophin complex functions as a scaffold for signalling proteins.* Biochimica et Biophysica Acta (BBA)-Biomembranes, 2014. **1838**(2): p. 635-642.

 doi:10.20944/preprints202511.0016.v2

3. Gao, Q.Q. and E.M. McNally, *The dystrophin complex: structure, function, and implications for therapy.* Comprehensive physiology, 2015. **5**(3): p. 1223-1239.
4. Hughes, D.C., et al., Age-related differences in dystrophin: impact on force transfer proteins, membrane integrity, and neuromuscular junction stability. Journals of Gerontology Series A: Biomedical Sciences and Medical Sciences, 2017. **72**(5): p. 640-648.
5. Duan, D., et al., *Duchenne muscular dystrophy.* Nature reviews disease primers, 2021. **7**(1): p. 13.
6. Vo, A.H. and E.M. McNally, *Modifier genes and their effect on Duchenne muscular dystrophy.* Current opinion in neurology, 2015. **28**(5): p. 528-534.
7. García-Rodríguez, R., et al., *Premature termination codons in the DMD gene cause reduced local mRNA synthesis.* Proceedings of the National Academy of Sciences, 2020. **117**(28): p. 16456-16464.
8. Mercuri, E., C.G. Bönnemann, and F. Muntoni, *Muscular dystrophies.* The Lancet, 2019. **394**(10213): p. 2025-2038.
9. Bies, R.D., et al., Human and murine dystrophin mRNA transcripts are differentially expressed during skeletal muscle, heart, and brain development. Nucleic acids research, 1992. **20**(7): p. 1725-1731.
10. Zhang, X.-f., W. Hu, and J. Hu, Neurological impairments in Duchenne muscular dystrophy: A comprehensive review. Acta Neurologica Belgica, 2025: p. 1-12.
11. Zhu, Y., et al., Serum enzyme profiles differentiate five types of muscular dystrophy. Disease Markers, 2015. **2015**(1): p. 543282.
12. Lo Cascio, C.M., et al., Gastrointestinal dysfunction in patients with Duchenne muscular dystrophy. PLoS One, 2016. **11**(10): p. e0163779.
13. Kutluk, M.G. and Ç.S. Doğan, Kidney involvement and associated risk factors in children with Duchenne muscular dystrophy. Pediatric Nephrology, 2020. **35**(10): p. 1953-1958.
14. Villa, C.R., et al., Identifying evidence of cardio-renal syndrome in patients with Duchenne muscular dystrophy using cystatin C. Neuromuscular Disorders, 2016. **26**(10): p. 637-642.
15. Klingler, W., et al., *The role of fibrosis in Duchenne muscular dystrophy.* Acta Myologica, 2012. **31**(3): p. 184.
16. Desguerre, I., et al., Endomysial fibrosis in Duchenne muscular dystrophy: a marker of poor outcome associated with macrophage alternative activation. Journal of Neuropathology & Experimental Neurology, 2009. **68**(7): p. 762-773.
17. Rozas, G. and J.L. Garcia, Drug-free evaluation of rat models of parkinsonism and nigral grafts using a new automated rotarod test. Brain research, 1997. **749**(2): p. 188-199.
18. Cendelín, J., I. Korelusová, and F. Vožeh, The effect of repeated rotarod training on motor skills and spatial learning ability in Lurcher mutant mice. Behavioural brain research, 2008. **189**(1): p. 65-74.
19. Kulesskaya, N. and V. Voikar, Assessment of mouse anxiety-like behavior in the light–dark box and open-field arena: role of equipment and procedure. Physiology & behavior, 2014. **133**: p. 30-38.
20. Wehling-Henricks, M., et al., Macrophages escape Klotho gene silencing in the mdx mouse model of Duchenne muscular dystrophy and promote muscle growth and increase satellite cell numbers through a Klotho-mediated pathway. Human Molecular Genetics, 2018. **27**(1): p. 14-29.
21. Çınar, R., et al., TRPM2 Channel Involvement in the Hesperidin-Mediated Potentiation of Cisplatin's Antitumor Action in Laryngeal Carcinoma Cells. International Journal of Molecular Sciences, 2026. **27**(3): p. 1141.
22. Solak, K., et al., Enhanced antitumor effects of interferon-stimulating DNA and magnetic hyperthermia in a breast cancer rat model. Journal of Drug Delivery Science and Technology, 2025. **110**: p. 107044.
23. Genc, S., et al., New Anti-Cancer Impact of Cerium Oxide, Lithium, and Sn-38 Synergy via DNA Methylation-Mediated Reduction of MMP-2 and Modulation of the PI3K/Akt/mTOR Pathway. Pharmaceuticals, 2025. **18**(11): p. 1725.
24. Sindhurakar, A., et al., An automated test of rat forelimb supination quantifies motor function loss and recovery after corticospinal injury. Neurorehabilitation and neural repair, 2017. **31**(2): p. 122-132.
25. Aartsma-Rus, A. and M. van Putten, *Assessing functional performance in the mdx mouse model.* Journal of visualized experiments: JoVE, 2014(85): p. 51303.
26. Shimizu-Motohashi, Y., et al., Restoring dystrophin expression in Duchenne muscular dystrophy: current status of therapeutic approaches. Journal of personalized medicine, 2019. **9**(1): p. 1.

 doi:10.20944/preprints202511.0016.v2

27. Taglietti, V., et al., Duchenne muscular dystrophy trajectory in R-DMDdel52 preclinical rat model identifies COMP as biomarker of fibrosis. Acta neuropathologica communications, 2022. **10**(1): p. 60.
28. Therapeutics, S., Sarepta Therapeutics Reports Positive Clinical Results from Phase 2 MOMENTUM Study of SRP-5051 in Patients with Duchenne Muscular Dystrophy Amenable to Skipping Exon 51| Sarepta Therapeutics, Inc.[Internet].(2021).
29. Happi Mbakam, C., G. Lamothe, and J.P. Tremblay, *Therapeutic strategies for dystrophin replacement in Duchenne muscular dystrophy.* Frontiers in Medicine, 2022. **9**: p. 859930.
30. Aartsma-Rus, A. and A.M. Krieg, FDA approves eteplirsen for Duchenne muscular dystrophy: the next chapter in the eteplirsen saga. Nucleic acid therapeutics, 2017. **27**(1): p. 1-3.
31. Mantuano, P., et al., β-Dystroglycan restoration and pathology progression in the dystrophic mdx mouse: outcome and implication of a clinically oriented study with a novel oral dasatinib formulation. Biomolecules, 2021. **11**(11): p. 1742.
32. Hack, A.A., et al., γ-Sarcoglycan deficiency leads to muscle membrane defects and apoptosis independent of dystrophin. The Journal of cell biology, 1998. **142**(5): p. 1279-1287.
33. Guhathakurta, P., et al., Enhancing interaction of actin and actin-binding domain 1 of dystrophin with modulators: Toward improved gene therapy for Duchenne muscular dystrophy. Journal of Biological Chemistry, 2022. **298**(12).
34. Wehling-Henricks, M., et al., Klotho gene silencing promotes pathology in the mdx mouse model of Duchenne muscular dystrophy. Human molecular genetics, 2016. **25**(12): p. 2465-2482.
35. Taghizadehghalehjoughi, A., et al., EVALUATION OF DYSTROPHIN ROLE IN DUCHENNE MUSCULAR DYSTROPHY-RELATED GASTROENTERITIS FOCUSING ON OXIDATIVE STRESS MECHANISM. Farmacia, 2025. **73**(5).
36. Welc, S.S., et al., Modulation of Klotho expression in injured muscle perturbs Wnt signalling and influences the rate of muscle growth. Experimental physiology, 2020. **105**(1): p. 132-147.
37. Suntar, I., et al., *Natural products, PGC-1α, and Duchenne muscular dystrophy.* Acta Pharmaceutica Sinica B, 2020. **10**(5): p. 734-745.
38. Lagu, B., et al., Selective PPARδ modulators improve mitochondrial function: potential treatment for duchenne muscular dystrophy (DMD). ACS medicinal chemistry letters, 2018. **9**(9): p. 935-940.
39. Handschin, C., et al., PGC-1α regulates the neuromuscular junction program and ameliorates Duchenne muscular dystrophy. Genes & development, 2007. **21**(7): p. 770-783.
40. Timpani, C.A., et al., Nitric oxide (NO) and duchenne muscular dystrophy: NO way to go? Antioxidants, 2020. **9**(12): p. 1268.
41. Theret, M., et al., *Macrophages in skeletal muscle dystrophies, an entangled partner.* Journal of Neuromuscular Diseases, 2022. **9**(1): p. 1-23.
42. Haenggi, T. and J.-M. Fritschy, Role of dystrophin and utrophin for assembly and function of the dystrophin glycoprotein complex in non-muscle tissue. Cellular and Molecular Life Sciences CMLS, 2006. **63**(14): p. 1614-1631.
43. Spencer, M.J., et al., Helper (CD4+) and cytotoxic (CD8+) T cells promote the pathology of dystrophin-deficient muscle. Clinical immunology, 2001. **98**(2): p. 235-243.
44. Deconinck, N. and B. Dan, *Pathophysiology of duchenne muscular dystrophy: current hypotheses.* Pediatric neurology, 2007. **36**(1): p. 1-7.